

# Flavor Production in Pb(160AGeV) on Pb Collisions: Effect of Color Ropes and Hadronic Rescattering

H. Sorge \*

Institut f. theoretische Physik, Universität Frankfurt  
Gesellschaft f. Schwerionenforschung, Darmstadt

## Abstract

Collective interactions in the preequilibrium quark matter and hadronic resonance gas stage of ultrarelativistic nucleus-nucleus collisions are studied in the framework of the transport theoretical approach RQMD. The paper reviews string fusion into color ropes and hadronic rescattering which serve as models for these interactions. Hadron production in central Pb(160AGeV) on Pb collisions has been calculated. The changes of the final flavor composition are more pronounced than in previous RQMD studies of light ion induced reactions at 200AGeV. The ratio of created quark pairs  $s\bar{s}/(u\bar{u}+d\bar{d})$  is enhanced by a factor of 2.4 in comparison to  $pp$  results. Color rope formation increases the initially produced antibaryons to 3 times the value in the ‘NN mode’, but only one quarter of the produced antibaryons survives because of subsequent strong absorption. The differences in the final particle composition for Pb on Pb collisions compared to S induced reactions are attributed to the hadronic resonance gas stage which is baryon-richer and lasts longer.

---

\*E-mail: [sorge@th.physik.uni-frankfurt.de](mailto:sorge@th.physik.uni-frankfurt.de)

# 1 Introduction

The ground state of quantum chromodynamics shows peculiar properties, confinement of colored degrees of freedom and spontaneous breaking of chiral symmetry. It is expected that at high temperatures and large baryon densities chiral symmetry gets restored and quarks are no longer confined. The central goal of modern heavy ion physics is to explore these properties of strongly interacting matter [1, 2]. Several experiments on nuclear targets are performed nowadays using the Au(11.6AGeV) beam at BNL or the Pb(160AGeV) beam at CERN. The first series of experiments with light ion beams (p,O,Si,S) has just been finished in these laboratories.

The work on which this paper is based has started some years ago [3]. The goal was set to develop a complete transport theoretical scenario of nucleus-nucleus reactions, from the initial state of two nuclei before overlap to the final state after the strong interactions have ceased (freeze-out). The developed model has been dubbed relativistic quantum molecular dynamics (RQMD). RQMD is a semi-classical microscopic approach which combines classical propagation with stochastic interactions. Strings and resonances can be excited in elementary collisions. Their fragmentation and decay leads to production of particles. Overlapping strings do not fragment independently from each other but form ‘ropes’, chromoelectric flux-tubes whose sources are charge states in higher dimensional representations of color  $SU_3$  [4]. The nature of the active degrees of freedom in RQMD depends on the relevant length and time scales of the processes considered. In low energy collisions (around 1 AGeV) RQMD reduces to solving transport equations for a system of nucleons, other hadrons and eventually resonances interacting in binary collisions and via mean fields (similarly to BUU [5], QMD [6], and so on). At large beam energies ( $> 10$  AGeV) the description of a projectile hadron interacting in a medium (in the simplest case a cold nucleus) as a sequence of separated hadron or resonance collisions breaks down [7]. A multiple collision series can be formulated on the subhadronic (quark) level. Following the paths of the ingoing constituent quarks, a Glauber-type multiple collision series is generated in RQMD, with cross sections taken from the additive quark model [8]. The secondaries which emerge from the fragmenting strings, ropes and resonances may interact with each other and the original ingoing hadrons (rescattering and mean-field interaction).

The RQMD model has been successfully applied to nuclear reactions at

ultrarelativistic energies (see e.g. [9]-[14]). The use of transport models like RQMD is not restricted to the study of the generated final state. It is of equal importance that such models can be used to study the influence of various types of interactions and medium effects on final state observables and to achieve a better insight into the *transient* stages of heavy ion collisions. Using the information from calculated RQMD events these questions have been addressed already in the literature, at 200A GeV mostly for S on A collisions [11]-[14]. Here and in a follow-up paper [15] I wish to expand on those results and study the amount of collectivity for central Pb(160A GeV) on Pb collisions. This is the heaviest projectile-target combination for which experiments are currently undertaken at CERN-SPS. Any kind of collectivity – physics of dense matter beyond mere superposition of independent nucleon-nucleon interactions – is expected to be strongest in a system with minimized surface-over-volume ratio. The paper presented here will focus on the influence of some important building blocks of RQMD – color ropes and hadronic rescattering – on the particle chemistry and distributions in phasespace. In particular, I shall consider the yields and momentum distributions of strange hadrons and antibaryons. Their production is dynamically suppressed in elementary hadronic interactions which makes them a useful probe for collectivity in the transient stage of AA collisions [16]. The follow-up paper mainly discusses the dynamical evolution of the created source in space-time until freeze-out.

The achieved degree of collectivity in the first – the prehadronic or quark matter – stage of nucleus-nucleus collisions is a central topic of heavy ion research. Soft multiparticle production is commonly described by fragmentation of excited color strings (see for reviews on this subject [19, 20, 21]). It is expected that independent string fragmentation, which means no collectivity at all, breaks down in central nucleus-nucleus collisions, because the string density gets too large. Interactions of overlapping strings is modeled as color rope formation in RQMD. Ropes can be viewed as a model of locally deconfined quark matter, which is dominated by longitudinal excitations and therefore of relevance for the preequilibrium stage in nucleus-nucleus collisions. The evolution in a rope is entirely governed by nonperturbative dynamics (a distance-independent rope tension). Other ‘second generation’ transport approaches also go beyond independent string fragmentation, for instance string fusion in QGSM [22], the Spanish version of the dual-parton model [23], or quark matter droplet formation in VENUS [24]. A common

result of these approaches is that strangeness and baryon pair production which is dynamically suppressed in elementary reactions becomes more favorable. On the other side, arguments have been put forward to include diquarks and an unsuppressed strange quark component into the nucleon sea ‘from the beginning’ which can be transformed into real particles by multiple collision effects[25].

Collectivity may also emerge in the hadronic stage of nuclear reactions, resonance matter formation – as studied in the models RQMD [26, 27] and ARC [28] – or mean fields [29, 30]. In recent years the interactions of resonances in a dense medium have found a lot of attention. For instance, resonances may act as ‘energy storage’ in multi-step collision processes which are of importance for heavy particle production [26, 31, 32]. Strictly spoken, there is no scattering ( $S$ ) matrix for resonances, because they are unstable. However, introducing them as quasi-particles makes sense under some limiting conditions ( $\Gamma/M \ll 1$ ). Note that resonance interactions can get important only in a system at sufficient density. The collision frequency has to be larger than the inverse of resonance lifetime (typically 1-2 fm/c).

The RQMD approach has evolved over the last years, because various interaction pieces have been put in step by step. After the important role of resonances had been recognized, a model was constructed for annihilation of mesons and baryons, including resonances, into nonstrange baryon resonances [26] and into a ‘string continuum’ [33]. Independent string fragmentation was replaced by color rope formation in case of overlapping strings [11]. Low energy hadronic interactions –  $s$  channel resonance formation,  $t$  channel meson and Reggeon exchange – have been modeled in the meson-meson [60] and the meson-baryon sector with net strangeness [14]. In this paper we are going to review these interactions in some detail. Some recent work to further develop the RQMD model for applications up to collider energies (multi-string excitations according to the AGK cutting rules [34]) will be described elsewhere [35].<sup>1</sup> These interactions have been implemented into the computer code RQMD (most recent version 2.1) which was developed by the author.

---

<sup>1</sup> For the topics of interest here multi-string excitations in  $NN$  collisions are of minor importance. On the one side, they tend to enhance the string densities. However, with respect to rope formation most of this effect is canceled at the comparably small CERN-SPS energy, because the average string length decreases in comparison to the case with 2-string excitations only.

## 2 Strings and ropes in $hh$ and $AA$ collisions

The so-called recombination approaches like RQMD assume that in elementary  $hh$  interactions the hadron wave function is decomposed into spectator and interacting quarks. The quark spectators neutralize their color while keeping their gluon cloud coherently bound (constituent quark picture). See Ref. [33] for a more detailed description. The interactions are dominantly initiated by slow quanta. The interacting constituent quark loses part of its gluon cloud, because the interacting components get out of phase with the spectator remnants in the cloud. These gluons form – together with their partners from the target – the source for secondaries. The parton language is used here rather loosely, to give a rough sketch of the process. There will be no attempt here to describe this process quantitatively by interactions of QCD quanta. It will be simply assumed that these interactions result in the longitudinal excitation of color strings. The concepts of strings in strong interactions actually predate QCD. There are many recent attempts to understand the properties of strings or equivalently chromoelectric flux-tubes directly from QCD, e.g. by invoking the dual Higgs mechanism for QCD-monopole condensation [17].

### 2.1 Strings in RQMD

In inelastic  $hh$  collisions the fraction  $x^+$  of the projectile lightcone momentum  $P^+ = E + p_l$  ( $p_l > 0$  assumed) which goes into target string excitation is determined from

$$dP \sim \frac{dx^+}{x^+} \quad , \quad (1)$$

with the lower limit set by the target hadron's (small) plus-component before collision. The target momentum (negative lightcone component) which goes into projectile string excitation is determined in the same way. This string excitation law is the same as originally suggested by the Lund group and realized in the Monte Carlo code FRITIOF [18]. The invariant masses of the target and projectile excitations should not fall below some minimum to allow for particle production. The minimum value is set to  $m+0.3 \text{ GeV}/c^2$ , with  $m$  usually taken as the ingoing hadron mass. Since the ingoing pseudoscalar mesons which are Goldstone bosons have exceptionally light masses,  $m$  is set in these cases to 0.7 (0.85) GeV for mesons without (with) strange valence quarks. The excited states decay either stringlike or – for excited

masses below some ‘smeared-out’ cut-off value ( $2 \text{ GeV}/c^2$  for nucleons) – as resonances.

The string topology generated in RQMD for  $hh$  interactions and displayed in fig. 1 is determined from the basic assumptions that all ingoing valence quarks keep on moving into the same direction and no net color flows between target and projectile. A sea quark pair gets polarized in course of the interaction resulting in spatial separation of sea quark charge and anticharge (see fig. 1). The interacting constituent quark combines with the sea anticharge into a colorless state. In the semi-classical picture the sea-quark companion starts to move backward due to the momentum flow from the target. Confinement forces the backward moving quark to pull out a string. The spectator quarks neutralize color in the same way as the interacting quark at the other end of the string. Of course, if energy is lacking the backward and forward sea-quark pair might be the same. In this case there will be no string, but decay of the created hadron excitation into two hadrons. In the terminology employed here a ‘color string’ (restricted to be a longitudinal excitation) is spanned between sea quarks which are identified with partons. Such a configuration is assumed to fragment in the same way into hadrons as a  $\bar{q}q$  configuration produced in  $e^+e^-$  annihilation. In contrast, the ingoing valence quarks are assumed to be ‘dressed’ (constituent quarks) and better prepared for hadronization. An ingoing spectator quark fragments differently (harder) than a partonic quark with equal momentum giving rise to the so-called leading particle effect. In the model quark spectators are able to transfer all their primordial momentum to the hadron(s) into which they fragment. The corresponding constituent quark structure functions are specified in [13, 33]. The interacting quark keeps only a fraction of its original momentum, in contrast to the spectator quark(s). The momentum which it keeps is dubbed  $p_B^+$  in fig. 1. The difference to the original momentum  $p_{Y_oY_o}^+$  is used up as the forward momentum of the excited string, i.e. for particle creation.  $p_B^+$  is determined stochastically using the string fragmentation function  $f(z)$  [19] as the probability measure. The backward momentum of the string  $p_{Ta}^-$  transferred from the target is determined from the equivalent of eq. (1). The decay properties of a color string are completely determined by its light cone momentum and the flavor at its end. The spectator momentum  $p_l^+$  does not enter at all into the calculation of the string evolution or its decay products. (see fig. 1).

The decay of elementary color strings into hadrons is calculated employ-

ing the concept of ‘left-right symmetric string fragmentation’ developed by the Lund group [19], with default JETSET 6.2 default parameters for  $f(z)$  [37]. The formation points of hadrons from string decay are calculated as the average of the two break points from which the quark constituents are emerging. This is schematically displayed in fig. 1 from which one can also read off the prescription for the formation points of hadrons containing one of the original valence quarks. In particular, the formation length of the leading hadrons coincides with the concept of so-called ‘constituent formation length’ [36] in which the formation length shrinks to 0 in the extreme limit  $z \rightarrow 1$ . The standard high energy 2-string scenario is modified in three cases, generation of additional strings from sea excitations which can be related to multi-Pomeron-exchange [38], projection of low-mass excitations onto resonance states and diffractive inelastic interactions [39].

Corrections to the 2-string-excitation scheme arise at lower energies, if the excited masses which are randomly chosen according to eq. (1) are below the cut-off values set for string fragmentation. If both outgoing states are below string excitation threshold, two hadrons (or resonances) are formed in the out-state

$$h_1 + h_2 \rightarrow h_1^* + h_2^* \quad . \quad (2)$$

Production of two baryon resonances is the dominating process in  $pp$  collisions at the AGS energies of 10 to 15 GeV. Furthermore, even at the highest beam energies strings are actually rarely produced in nonannihilating events during the rescattering stage of nucleus-nucleus collisions. Therefore production (and absorption) of resonances in  $2 \rightarrow 2$  processes effectively replaces the 2-string excitation component and fills up the inelastic cross section, in addition to  $s$  channel resonance formation and meson exchange processes in the  $t$  channel (see section 3).

Let us assume now that above condition leading to a reaction of the type in (2) is met. The two produced excitations have to be projected onto hadronic states. Resonances are propagated explicitly in RQMD and may scatter themselves. All lightcone momenta which enter into eq. (1) are calculated as if the ingoing hadrons would be groundstate hadrons, keeping the CMS energy the same. Thus the class of out-channels in (2) is populated with the same probability and cross section (given the same total cross section), irrespectively whether  $h_1$  and  $h_2$  are excited states or not. The need to respect detailed balance requires some modifications which were neglected in

earlier versions of the RQMD model [26]. The improved model for such  $2 \leftrightarrow 2$  transitions will be described in the following. The flavor of each hadron is kept the same, an assumption which can be dropped eventually in further refinements of the model to allow for flavor-exchange between the collision partners. The out-channel is chosen randomly with proper weights to give the following cross sections for  $2 \leftrightarrow 2$  where each term in the sum corresponds to the production cross section of a particular 2-hadron (resonance) state:

$$\sigma(k, l \rightarrow '2') = \sigma_0(s) \sum_{i,j} p_{ij}^2 \quad (3)$$

$$(2S_i + 1)(2S_j + 1) \cdot SF(kl, ij) \quad .$$

$i-l$  label hadron states,  $p_{ab}$  denotes the CMS momentum and  $S_a$  the spin of hadron  $a$ .  $\sigma_0(s)$  is determined by the normalization condition. Depending on the initial choice – a nondiffractive or a diffractive inelastic interaction – the sum runs over all allowed states  $i$  and  $j$  or is restricted by the constraint that either hadron  $i$  or  $j$  is a groundstate hadron.  $SF(kl, ij)$  denotes a symmetry factor which is unequal to 1 only for  $k \neq l$  and  $i = j$ . In this case it is 1/2 to respect the detailed balance relation. Since eq. (3) is implemented in RQMD employing the Monte Carlo technique, the transition  $kl \rightarrow ii$  is assigned first a probability which ignores the symmetry factor. Afterwards the transition is accepted with probability 1/2. In case of rejection an elastic collision is realized. The physics content of eq. (3) is rather simple. The out-states are chosen according to phase space and available spin degrees of freedom, its functional form in accordance with the detailed balance relations. The basic idea is that statistics governs the population of out-states if many states are available in binary collisions.

Extending the RQMD approach from  $hh$  to  $hA$  and  $AA$  collisions by allowing for multiple string excitations is straightforward. Each nondiffractive constituent quark interaction generates a new string if the energy is sufficient [13]. The cross section of interacting constituent quarks is given from the additive quark model  $\sigma_{q-q} = 1/9 \cdot \sigma_{NN}$  which keeps the original projectile cross section constant while the projectile is traversing the target. Multiple interactions can be pictured as continuing ‘undressing’ of a constituent quark propagating through the target.

It is an important question for the degree of baryon stopping and the achievable baryon densities in nucleus-nucleus reactions how the baryon num-



ber is shifted in multiple nucleon collisions with a target. The minimal-stopping approach is to concentrate all momentum which is not used up for target string excitation into a leading diquark which fragments like in a  $NN$  collision. Historically, this was the first approach which has been applied in string fragmentation models [40, 41]. It is well-known by now that the minimal-stopping approach is at variance with the experimental data in ultrarelativistic  $pA$  and  $AA$  collisions [42]. The shift of baryon number in rapidity is stronger. It contains a component which goes with the number of additional projectile collisions. In the beginning several people have parametrized the dependence of the nuclear stopping power as a function of the number of additional collisions [43]. A model for baryon stopping which contains a strong dependence on the number of collisions was suggested in [33] and is applied in RQMD. It is in good agreement with available baryon measurements of the NA34, NA35 and NA44 group in 200A GeV collisions [13]. In this approach the light cone momentum fraction of the baryon after fragmentation is determined from the number of spectator constituent quarks which it keeps in its wave function. The topology of string excitations in multiple baryon collisions and the distribution of the ingoing momentum between the active degrees of freedom (strings and constituent quarks) are displayed graphically in fig. 2. Each further inelastic interaction in a target removes an additional constituent quark from the spectator remnant replacing it by a sea quark with zero momentum (in this approximation). It may even happen that none of the original constituent quarks ends up in the outgoing baryon. In this case a partonic sea diquark moves at the forward end of one of the projectile strings, and the baryon momentum is determined from string fragmentation.

The ingoing hadrons are complex objects themselves. Multiple collisions of a hadron at high energy are not sequential collisions of a single object, but in each collision a different hadron component is involved. Simple consideration of time scales tells that multiple soft interactions of the same object are highly suppressed. A fast particle which needs on the order of 1 fm/c in its rest system to finish the first interaction has left the target far behind which suppresses a subsequent interaction. This argument can be given a more rigorous meaning by analysing planar diagrams with multiple ‘ladder’ exchange [44]. Using the same line of argument multiple quasi-elastic collisions ( $2 \rightarrow 2$ ) and inelastic diffractive interactions should be suppressed as well at high energies. Of course, the basic reason behind the suppression of multiple

collisions within short time intervals is of quantum-mechanical nature. The uncertainty relation associates a finite time and distance interval to an interaction which can be characterized by exchange of energy and momentum. Recently a first step was done to take this effect into account in RQMD. Since the particle propagation in RQMD is realized semi-classically, only an approximate solution can be found in this framework. It was discussed a long time ago by Low and Gottfried that a classical space-time concept of propagation can be applied for fast particles [45], because rapidity and longitudinal position are commuting in this limit. Therefore one is allowed to specify  $z$ ,  $t$  and  $y$  after a collision. The space-time interval after which a quasi-elastic or diffractive collision is considered as finished is now defined by

$$x_{min}^+ = x_{Coll}^+ + \Delta x^+ \quad , \quad (4)$$

assuming that the particle is moving in forward ( $=+$ ) direction. (A corresponding relation holds for the collision partner.) If the collision cannot be finished before the next collision is going to take place, the first collision being ‘too soft’ is discarded. The collision point  $x_{Coll}$  is defined from the minimum distance value which the two classical hadron trajectories can have in their 2-body center of mass frame.  $\Delta x^+$  is calculated using

$$\Delta x^+ \sim 1/\Delta p^- \quad , \quad (5)$$

with  $\Delta p^-$  the absolute value of the lightcone momentum which the hadron has picked up from the collision partner. (As usual in RQMD the longitudinal component is defined in the 2-body CMS by the direction of particle motion before collision.) Relation (5) is motivated by the Heisenberg relation  $\Delta x^+ \cdot \Delta p^- \geq 1$ . The proportionality factor is presently set to 1. Applying the criterion of relation (5) to all 2→2 collisions which are generated by RQMD in the dynamical evolution of nuclear collisions suppresses soft collisions. By their very definition, not many particles are produced in such collisions. Therefore the resulting effect on the final particle yields is small in A(200AGeV) on A collisions, on the few percent level. The quantum-mechanical suppression of very soft multiple collisions in AA interactions at other beam energies is currently studied. The results will be presented elsewhere.

## 2.2 Color ropes in RQMD

The quarks which have been polarized from the sea in course of the initial interactions are receding from each other. Their masses are usually small compared to their lightcone momenta and neglected. Therefore these quarks are moving on the lightcone and form the sources of the chromoelectric field filling the region between the forward and backward moving charges. The field is compressed into tubes with the tube cross section kept independent from the field strength. Thus a collection of tubes is spanned in  $AA$  collisions.

First, I am going to describe the physics of a single chromoelectric flux-tube. The formation of tubes with stronger than the elementary string fields could be of relevance for  $AA$  collisions but also for soft multiparticle production in hadron-hadron collisions at collider energies [46]. The created  $SU(3)$ -valued color fields inside each tube are added coherently. The elementary triplet charges of quarks and antiquarks in one of the receding rope ‘condensator’ plates are coupled stochastically to the total  $SU_3$  color charge as the source of the rope field:

$$(p, q) \otimes (1, 0) \rightarrow (p + 1, q) \oplus (p - 1, q + 1) \oplus (p, q - 1) \quad , \quad (6)$$

with the statistical weight given from the dimension of each multiplet

$$d(p, q) = \frac{1}{2} \cdot (p + 1) \cdot (q + 1) \cdot (p + q + 2) \quad .$$

The possible couplings of an arbitrary  $SU_3$  charge with an elementary charge are graphically displayed in fig. 3.

The chromoelectric field of the rope is determined in the flux-tube picture by Gauss’ law:

$$E^\alpha(p, q) \cdot A(p, q) = g F(p, q)^\alpha \quad . \quad (7)$$

$(p, q)$  characterizes the multiplet of the QCD charge.  $F(p, q)^\alpha$ ,  $\alpha = 1, 8$  are the generators of the  $SU(3)$  group in the corresponding representation. It follows that the energy density of a rope field is proportional to the eigenvalue of the Casimir operator  $C(p, q) = F(p, q)^\alpha \cdot F(p, q)^\alpha$ . In RQMD the transverse size of a rope  $A(p, q)$  is being kept independent on the representation of the source. This is required in the flux-tube model to get scaling of the rope tension with the Casimir eigenvalue which has been observed for both  $SU_2$  and  $SU_3$  gauge groups [47]. Thus the rope tension, the energy per unitlength, also scales with the Casimir eigenvalue

$$\kappa(p, q) = 3/4 \cdot C(p, q) \cdot \kappa_{el} \quad . \quad (8)$$

The tension of a triplet flux-tube (elementary string)  $\kappa_{el}$  can be related to the Regge slope parameter  $\alpha'$  which gives 0.9 GeV/fm. It is well-known that the flux-tube picture emerges from QCD with static quarks in lowest order of the strong coupling expansion [48]. Recently the assumed flux-tube properties – dominance of the longitudinal electrical field components, scaling of the field strength with  $C(p, q)$  and charge independence of the transverse extension of the field – have been confirmed by a calculation of Wilson loops for higher dimensional charges in 3-dimensional  $SU_2$  lattice gauge theory [49]. Note that these new lattice results provide important information concerning the dynamics underlying confinement. If confinement is due to a bulk property of the QCD vacuum (like as the pressure in bag models), then the transverse size of higher dimensional flux-tubes is expected to increase. Consequently, the rope tension would scale less rapidly, as the square root of the Casimir eigenvalue only. Thus phenomenological models of confinement like the bag model are not compatible with the recent results of lattice simulations.

Quark-antiquark pairs are created from the chromoelectric field and screen the original field [51]. In a first approximation the total pair creation rate and the flavor composition can be calculated employing Schwinger’s vacuum persistence rate for a constant electric field [50]. This is done by treating the pair creation as a tunneling process in the semi-classical WKB approximation (see Appendix). Employing a local density approximation, the calculated pair creation rate determines stochastically the space-time points in which the field strength is degraded by created quarks. This procedure generalizes the Artru-Mennessier scheme [52] to the situation of fields with variable strength. Of course, some modifications of the decay probability are expected for very short times [53] and near to the sources of the rope field [54]. The pair creation probability per unit time and length is obtained by integrating over the transverse rope area  $\pi \cdot r_{tube}^2$  with transverse rope radius set to 0.8 fm. The radius parameter is fixed by the requirement to get reasonable production rates from elementary string decays in comparison to  $e^+e^-$  hadroproduction data. Strange quark production is easily enhanced by increasing the field strength, because the mass difference between the light flavors becomes irrelevant for sufficiently large fields. In contrast, 3-diquark creation inside the rope stays rather weak in the average. The small probabilities to create a diquark pair by the rope field have their root in the assumed 2-step process as outlined in Ref. [13].

The collective field is gradually degraded, because the initial ‘macro-

scopic' spatial separation of charge and anticharge cannot be maintained. The first mechanism to degrade the field strength is quark pair production. Pair creation points, the created flavor and transverse momenta are sampled stochastically. The local field strength is calculated self-consistently, taking screening of the original field by already produced quark pairs into account. The rope tension is lowered in the forward lightcone of each break point from  $\kappa(p, q)$  to  $\kappa(p', q')$ . E.g.,  $(p', q')=(p, q - 1)$  if a quark is pulled out of the vacuum and attracted by the charge  $(p, q)$ .

There are two other processes which degrade the original field strength, turning points of quarks in the rope end plate and crossing points of two color charges inside the rope. All these processes are displayed together in fig. 4. The turning point of a quark is determined from the condition that its original momentum has been used up by propagating under the force of the rope. Its momentum loss per unit-time is given from

$$\frac{dp}{dt} = \pm \frac{\kappa(p, q)}{p + q} \quad (9)$$

with the sign depending on the direction of motion. Of course, this is the direct generalization of the situation in string decay to account for the finite total momentum. Using eq. (9) independent fragmentation is recovered in the limit that the fragmentation products of two strings have no overlap in rapidity space.<sup>2</sup> In this case the initial quark momenta show complete mismatch, e.g. one string is specified by  $(P^+, \delta^-)$ , the other by  $(\delta^+, P^-)$  with  $\delta^{+,-} \ll P^{+,-}$ . The region with non-triplet field strength shrinks to zero for  $\delta^{+,-} \rightarrow 0$  and  $P^{+,-} \rightarrow \infty$ . Similarly, those parts of string world sheets which do not overlap with other strings can make no contribution to build up a region of larger field strength. In RQMD these nonoverlapping parts of generated strings are split off from the beginning in the rope fragmentation process. The reason is the following. As displayed in fig. 3 two quarks (anti-quarks) may coalesce into a diquark in the  $\bar{3}$  ( $3$ )-representation during the process of rope charging. Guided from the general coalescence picture one might expect that such a diquark would break if the momentum mismatch is too large between the two constituents, and an additional meson would be created. I have checked by introducing a 'reasonable' parameter for diquark break-up

---

<sup>2</sup> The hadron rapidity distribution from string fragmentation is approximately constant within some limits  $y_{min,max}$ . The limits are related to the energy-momentum of the string via the relations  $y_{min,max} \approx \ln P^{-,+} - \ln(2m)$ , with  $m$  a typical hadron mass.

that practically the same results are achieved from rope fragmentation as in the parameter-free default procedure.

The third process of field degradation, crossing trajectories of two color charges which do not form a singlet, has no analogue in an elementary string decay. It had also not been considered in early studies of the materialization time after which the rope field is degraded to zero [55]. The two crossing charges need not form a white state as long as there are other color charges available which can neutralize their charge (see fig. 5). Of course, two triplet or two antitriplet charges always cross without being able to form a color singlet. The probability that quark and antiquark form a white state is given in the model as  $(1+p' \cdot q')^{-1}$ , with  $p'$  ( $q'$ ) being the number of 3 ( $\bar{3}$ ) charges available to neutralize the antiquark (quark) charge after crossing. This probability becomes very small for regions of high field strength. Thus color is confined globally in a rope, but not locally. In contrast, color charges are neutralized always locally in a fragmenting string.

The quark pairs are produced in a rope with zero longitudinal momentum, but afterwards they are accelerated in the force field of the outer charges (see fig. 5). The accelerating force is given by the difference between the rope tensions before and after pair production  $\kappa - \kappa'$ , the same force which is driving the pair creation process. The classical trajectories are calculated neglecting the finite quark masses as it is usually done for string fragmentation. Therefore all charges are moving with the velocity of light all the time. This simplifies the calculation considerably and is, in fact, the only lorentzinvariant propagation without reference to the global rope rest system.

Finally, all original and newly produced quarks will end up in a color singlet with a corresponding partner. The color singlets are projected onto the basic hadron multiplets, with the same relative weights as for string fragmentation. The generation of three-quark systems and projection on baryon states require some care [14]. Independent choice of three quark flavors in the rope endplates tends to overpopulate baryons with quarks of unequal flavor. Thus each chosen configuration is assigned a proper weight to avoid an unphysical flavor  $SU_6$  breaking. The positions of the breakpoints are slightly readjusted that all hadron momenta which are determined from the momentum sum of their constituents fulfill the mass shell constraints. The whole rope fragmentation scheme is constructed in a way that total net flavor and energy-momentum are conserved. The hadron formation points are calculated from the quark trajectories. A formation point is defined

defined by

$$x_h^\pm = x^\pm(\text{Yo-Yo}) - p_h^\pm/(2\kappa_{el}) \quad , \quad (10)$$

where  $x^\pm(\text{Yo-Yo})$  is the first meeting point of the two quark constituents forming a hadron with momentum  $p_h^\pm$ . In case of a triplet charges as the source of the rope field this prescription reduces to the corresponding definition of formation points in string decay (cf. fig. 1).

It is clear from relations (6) that in the process of rope charge formation a triplet and an antitriplet charge may eventually form a color singlet and do not contribute to the total rope charge (see also fig. 3).<sup>3</sup> In the most extreme case the total charge is zero and the region of the rope is field-free! The probability that this may happen is rather small, however [4]. The quarks which form a color singlet in the rope endplates are projected onto hadron states of the basic flavor  $SU_3$  multiplets. The momentum of such a hadron is given from the sum of the quark light cone momenta (if the hadrons are assumed massless, in the real calculation up to a small correction). The hadron formation point cannot be determined from the rope dynamics to which the quark constituents do not contribute in this approximation. It is usually expected that formation point and momentum are related in soft production processes, approximately  $x^\pm \sim p^\pm$ , which is used here with the scale factor  $\kappa_{el}$ .

The fragmentation of a single color rope as it is implemented in the RQMD model has just been described. In this picture several flux-tubes are formed in very energetic  $AA$  reactions which may cover the whole transverse area of overlap between the two ingoing nuclei. How is the fusion of strings into several ropes realized in RQMD? At first the strings are generated independently. The hadronization of each string is calculated in a Monte Carlo-type fashion, and the information is stored. This decay is considered as ‘virtual’ until a first ‘would-be’ hadron of a decayed string is emerging at its formation point. All other strings which have been generated so far are now examined whether the transverse coordinates of their origin have a smaller distance to this first string than the flux-tube radius  $r_{tube}$ . ‘Transverse’ and ‘longitudinal’ refers to the coordinates in the rest system of this string. Thus the specification of the fusion process is lorentz invariant. Of course, the

---

<sup>3</sup> This process was neglected in the first RQMD calculations which included rope formation [11]. It changes the results from rope fragmentation on the order of 5 %, because the probability to form a color singlet by statistical combination of 2 randomly chosen (anti-)triplet charges is 1/18.

longitudinal direction coincides usually approximately with the beam direction. Furthermore, it is checked whether the world sheets which are swept out by each  $Q\bar{Q}$  pair during half a period of string motion overlap in the  $t$ - $z$  plane. Note that this criterion is trivially satisfied at asymptotic energy, because all string origins will be identical in this case. If no other string is found which fulfills the criteria the string decay is considered as ‘real’ and all hadrons emerging from its fragmentation are propagated subsequently. All strings which have been accepted are collected, and their independent decay is rejected. Instead, they fuse into a rope.

In principle, the interactions between flux-tubes can be more complicated than in the model adopted in RQMD, e.g. transverse ‘communication’ between different tubes. So far such interactions are not taken into account. It should be noted, however, that the recent lattice results [49] provide some justification for neglecting these interactions in a first approximation. Trotter and Woloshyn have shown that the color ropes in lattice gauge theory do not expand in transverse dimensions. This result has been obtained in the static limit, with an infinite amount of time available and with only the nonperturbative vacuum outside the tube.

The need to go beyond independent string fragmentation for an understanding of the early stage in ultrarelativistic AA collisions is generally accepted nowadays. Of course, the appropriate replacement by more sophisticated approaches in line with QCD is currently under debate. It should be added that the string fusion approach of Refs. [22, 23] based on the dual parton model is similar to the concept which is realized in RQMD. A major difference is that in the DPM calculations only fusion of at most two strings is considered so far. Fused strings break only as a whole in these DPM Monte Carlos while in RQMD stepwise field degradation is introduced. The RQMD approach seems better suited in case that many strings overlap and fuse. Nevertheless, possible effects of a different fragmentation procedure could be compensated partially modifying the fusion strength. A direct comparison of results from the two string fusion approaches which will be undertaken later on shows rather similar trends for central Pb on Pb collisions at CERN-SPS energy. The beam energy may be too low that single-particle observables display sizable sensitivity to details of string fusion based models.



### 3 $hh$ interactions in the rescattering stage

The interactions in the hadronic resonance gas stage are described by binary collisions between hadrons. Although preequilibrium processes are present in  $AA$  collisions [13], the interactions are usually of nonasymptotic type, in the energy region of resonance production, formation and absorption. Most of the work in the RQMD framework has been devoted to develop a reasonable model for all so-called nonexotic reactions. In these reactions an  $s$  channel resonance can be formed as an intermediate state. A basic motivation is that the interaction strength is much larger here. (The energy-momentum entering the denominator of the corresponding  $T$  matrix element can be near to a pole.) Experimental justification comes from large differences of cross sections in nonexotic versus exotic channels, e.g.  $\bar{K}N$  versus  $KN$  or  $\pi\pi$  with isospin 0 or 1 as compared to isospin 2, at low and medium energies. If ingoing hadrons form a state with quantum numbers not allowed for a single hadron by the quark model (exotic state), the low and medium energy interaction is solely given by  $t$  channel hadron (Reggeon) exchange. Only nonexotic reactions do allow quark-antiquark annihilation in the entrance channel. This process is very important for the flavor dynamics in  $AA$  collisions. If the system starts with strangeness below chemical equilibrium values, quark-antiquark annihilation in nonexotic reactions drives the system towards chemical equilibration. Therefore this section presents a detailed description of the RQMD model for the nonexotic reactions. A modeling of these processes is clearly needed, because hadronic resonances which are treated as quasi-particles may interact themselves. For strangeness creation these processes are actually much more important than the interactions solely between groundstate hadrons. <sup>4</sup> It was a very early observation in hadron physics that bumps show up in the energy dependence of cross sections which can be identified with the excitation of discrete Breit-Wigner type resonance states, e.g. the  $\Delta(1232)$ . Hadronic interactions at somewhat larger energies are dominated by quark exchange and annihilation (describable as Reggeon exchange) whose energy dependence are given by a negative power of  $s$ . At even higher energies Pomeron exchange in elastic interactions – exhibiting

---

<sup>4</sup> For instance,  $\pi N$  interactions are insufficient to explain the  $\Lambda$  and  $K$  enhancement in S induced collisions at 200A GeV, in contrast to e.g. the conjecture in Ref. [25]. The strangeness suppression in  $\pi N$  collisions at the relevant invariant mass above 1.6 GeV/c is rather similar to  $pp$  collisions at 200A GeV.

some kind of universality – induces an approximately energy independent total cross section for hadron-hadron collisions. These three components – with their characteristic and different energy dependences – can be identified with three pieces of interaction in RQMD: formation of discrete resonance states, annihilation into a resonance or string ‘continuum’ and excitation of two (or more) strings which was described in the section before. The importance of each component varies for different hadronic reactions. Four classes of interaction can be distinguished according to the number of ingoing (anti-)baryons ( $B$  denoting baryon,  $M$  denoting meson):  $BB$ ,  $BM$ ,  $MM$  and  $\overline{B}B$ . The charge reversal invariance of strong interactions can be used to generate all other interactions of antibaryons.  $MM$  and  $MB$  interactions in states with nonexotic quantum numbers get some contribution from each component. In contrast,  $B\overline{B}$  annihilation may occur only in the continuum, because the minimum invariant mass is too large.

A description of the interactions which are induced by quark exchange and annihilation has to interpolate smoothly from the low energy region of  $s$  channel resonance formation to the high energy interactions which are better described in terms of  $t$  channel Reggeon exchange. Of course, the old discussion about ‘duality’ of these two descriptions has never lead to satisfying results [56]. For the construction of the  $hh$  interaction in RQMD related to quark annihilation and exchange I follow a pragmatic approach, adding together a few lowlying resonances and a Regge-type parametrization. The formation of  $s$  channel resonances is calculated in the  $MB$  and the  $MM$  sector from multichannel Breit-Wigner formulae. It is assumed for RQMD that resonance formation determines completely the interactions in nonexotic channels up to some CMS energy  $\sqrt{s_0}$ . This statement is not completely true as will be explained lateron. (There are some small corrections due to  $t$  channel background processes.) Above  $s_0$  when a description in terms of discrete resonance levels becomes invalid – the ‘annihilation’ cross section (for  $\pi\pi$ ,  $\pi N$ ,  $\overline{K}N$ , etc.) is assumed to decrease with energy as  $1/\sqrt{s}$ . Since the tails of the Breit-Wigner resonances decay much faster with energy, the resulting gap to the total annihilation cross section ( $\sigma_{Ann}$ ) is filled by annihilation into a ‘continuum’ which serves as the bridge to Reggeon exchange, at high energy supposedly dominant over  $s$  channel resonance formation.<sup>5</sup>

---

<sup>5</sup> The cross section related to Reggeon exchange is dubbed here ‘annihilation’ cross section for terminological convenience, though part of the physics may really be quark ‘exchange’. I shall come back to this point later.

The choice of the exponent  $-1/2$  for the power of  $s$  in the energy dependence of  $\sigma_{Ann}$  is motivated by the existence of energy thresholds in  $2 \rightarrow 3, 4, \dots$  reactions. They can be described by multiple Reggeon exchange [56] and effectively increase the maximum value  $-1$  for the power of  $s$  in  $2 \rightarrow 2$  Reggeon exchange processes as determined from the  $\rho$  trajectory (and, of course, from experimental data). One can test the assumed energy dependence by looking at reactions which are tied to Reggeon exchange and *not* to high energy processes determined by Pomeron cuts. For instance, the energy behaviour of the inclusive cross section  $K^- p \rightarrow \Lambda + X$  – one of the rare cases in which flavor tagging allows for rather good distinction – is consistent with  $1/\sqrt{s}$  in the relevant energy region ( $s > 4\text{GeV}^2$ ).

Since the annihilation cross section decreases with energy, a gap to the total cross section ( $\sigma_{tot}$ ) opens up.  $\sigma_{tot}$  is either given from experimental data or calculated using the additive quark model [33]. The physics filling the gap is the high energy component of  $hh$  interactions, Pomeron exchange for high energy elastic interactions and Pomeron cuts in inelastic collisions [34]. It follows from the considerations above that the energy dependence of the high energy component in reactions with *measured* total cross sections (e.g.  $\pi N$ ,  $\bar{K}N$ ) turns out to be approximately proportional to  $(1-\sqrt{s_0/s})$ . This functional dependence on energy is used to switch on the high energy component of the total and elastic AQM cross sections for reactions with unmeasured cross sections.

After the general idea has been presented how the annihilation cross sections are constructed as a sum of Breit-Wigner and continuum contributions, I am going to discuss the various classes of reactions specifically. The general scheme is realized somewhat differently in different channels depending on the level of experimental knowledge.

### 3.1 Formation of $s$ channel resonances

Let us turn first to meson-meson interactions. Each of the three vector mesons  $\rho(770)$ ,  $K^*(892)$  and  $\phi(1020)$  decays into two pseudoscalar mesons. It is experimentally well-known that  $\rho(770)$  and  $K^*(892)$  dominate the phase-shifts in the  $p$  wave for  $\pi\pi$ ,  $I=1$  and  $\pi K$ ,  $I=1/2$  scattering and can be described well by isolated Breit-Wigner resonances above a small background. The formation of these 3 and 26 additional meson resonances in the mass region up to  $1800 \text{ MeV}/c^2$  is taken into account in RQMD. Note that not

all  $SU_3$  flavor nonets are complete due to lack of experimental information about resonance masses and widths. However, all lowlying multiplets – the scalar, the two axial vector and the tensor mesons – are completely included. The groundstate mesons and the resonances of these multiplets are propagated explicitly in RQMD, while the other resonances do appear only in the intermediate states.

Godfrey’s and Isgur’s quark model calculation [57] which is rather successful in explaining measured branching ratios of resonance decays has been taken to extract resonance couplings to unmeasured decay channels. Partial decay widths of resonances which can decay only off-shell into a  $\phi$ , have been related to measured branching ratios employing flavor  $SU_3$  symmetry and a correction for phasespace kinematics. This applies to the  $K^*$  resonances of the lowlying tensor and two axial vector nonets.

In RQMD Breit-Wigner type multi-channel cross sections for  $s$  channel resonance formation are usually summed up incoherently. Exceptions are  $\pi\pi$ ,  $I=0$  and  $\pi K$ ,  $I=1/2$  reactions in the  $s$  wave. Here interferences are taken into account, because very broad resonances are present in these channels ( $f_0(1400)$  and  $K_0^*(1430)$ ) which interfere with a strong background from attractive interactions [58]. In addition, the narrow  $f_0(975)$  state interferes destructively in the scalar-isoscalar channel with the other  $f_0$  resonance and a background. The phases of resonances and background are added in the elastic channels

$$\delta_0 = \delta_b + \sum_R \delta_R \quad , \quad (11)$$

which is the appropriate way to get an unitary  $S$  matrix as long as only one channel is open. The background phase  $\delta_b$  can be calculated from one-meson exchange in the  $t$  channel employing the  $K$  matrix formalism (see the subsection 3.3).  $\delta_R = \arctan\left(\frac{\Gamma_{el}/2}{m_R - \sqrt{s}}\right)$  is the phase attributed to each resonance. In particular, unitarity is important for the  $\pi\pi$  interaction in the scalar-isoscalar channel. Just below invariant mass of 1 GeV the phaseshift goes through 180 degrees due to the strong destructive interference effects. If more than one channel opens up with increasing energy (in  $\pi\pi$  interactions the  $K\bar{K}$  channel), the situation becomes even more involved. In order to ensure continuity of the  $S$  matrix across the thresholds eq. (11) is also used above particle production threshold. The inelasticity parameter  $\eta$  in the diagonal elements of the  $S$  matrix  $S_{ii}^J = \eta_i \exp(2i\delta_i)$  is calculated from the

unitarity condition

$$\sum_k S_{ki}^{J*} S_{ki}^J = 1 \quad (12)$$

with the (small) non-diagonal elements given from addition of Breit-Wigner-type  $T$ -matrix elements. No relative phase between resonances and background is introduced which would allow the construction of a completely unitary multi-channel  $S$  matrix. This is possible in the framework of the Davies-Baranger formalism [59]. The results in the scheme adopted here and in this more complicated unitarization approach are rather similar, however [60].

In all meson-baryon interactions with quantum numbers allowed for a baryonic state from flavor  $SU_3$  resonances may be formed. So far, however,  $\Omega^*$  formation is neglected in RQMD. The properties of nonstrange baryon resonances – with isospin 1/2 ( $N^*$ ) and 3/2 ( $\Delta^*$ ) – have been experimentally well explored in  $\pi N$  collisions, and of hyperon resonances (with isospin 0 and 1) in  $\bar{K}N$  interactions. The knowledge about multiply strange baryon resonances ( $\Xi^*$  and  $\Omega^*$ ) is poor, however. A generalized Breit-Wigner formula for the cross section is used to calculate the  $s$  channel resonance formation probabilities (for  $N^*$ ,  $\Delta^*$  and  $\Xi^*$ ):

$$\sigma_{MB \rightarrow B^*} = b(s) \cdot \frac{\pi}{p^2} \cdot \sum_R \frac{(2J_R + 1)}{(2S_1 + 1)(2S_2 + 1)} \cdot \frac{\Gamma_R(MB) \cdot \Gamma_R(\text{tot})}{(\sqrt{s} - m_R)^2 + \Gamma_R(\text{tot})^2/4} \quad (13)$$

$b(s)$  is a normalization factor which renormalizes – for  $N^*$  and  $\Delta^*$  formation – the Breit-Wigner sum to a given absolute cross section. (For  $\Xi^*$  formation incoherent addition gives  $b(s)=1$ .) The renormalization is done for nonstrange baryon resonances, because the total cross sections in  $\pi N$  reactions are known. The total resonance formation cross section calculated with eq. (13) in  $\pi N$  is actually the total  $\pi N$  cross section minus an elastic background (up to 5 mb) determined by a consistency condition that the sum of background and elastic resonance decay equals the measured elastic  $\pi N$  cross section.  $\Gamma_R(MB)$  denotes a partial decay width into the channel with meson  $M$  and baryon  $B$ . The decay widths are  $\sqrt{s}$ -dependent via the relative momentum in the CMS of the decaying resonance  $p$

$$\Gamma_R(MB) \sim m_R/\sqrt{s} \cdot p^{(2l+1)} / (1 + 0.2 \cdot (p/p(m_R))^{2l}) \quad (14)$$

This ensures a correct threshold and high energy behaviour of a particular channel. The particular resonance which is formed in a meson baryon anni-

hilation is chosen randomly with a weight given by the corresponding term in the sum of eq. (13).

In the  $N^*$  and the  $\Delta^*$  channel the sum in eq. (13) runs over all resonances with a mass below  $2 \text{ GeV}/c^2$ . The resonance masses and decay parameters as implemented in RQMD <sup>6</sup> are in accordance with the listing of the Particle Data Group [61]. It has been checked that an application to  $\pi N$  collisions reproduces approximately the hyperon-kaon production cross sections and the total pion yields in inelastic collisions [33].

In the  $\Xi^*$  channel formation cross sections for 6 discrete resonance states are incoherently added with couplings to meson-baryon states given from  $SU_3$  flavor symmetry. (Note that flavor  $SU_3$  is broken by different  $M$  and  $B$  masses in each octet.) The  $F$  and  $D$  parameters specifying the strength of symmetric and antisymmetric coupling are taken from the literature [62].

Resonance formation as given in eq. (13) is not realized for hyperon resonance formation ( $\Lambda^*$  and  $\Sigma^*$ ). Instead, the experimentally measured exclusive cross sections for charge exchange ( $K^- p \leftrightarrow \bar{K}^0 n$ ), elastic interactions and hyperon production ( $\bar{K}N \leftrightarrow \pi\Lambda/\pi\Sigma$ ) have been tabellized in RQMD. The  $\Sigma^*$  resonance parameters are not determined very well. Furthermore, at low energy the  $\bar{K}N$  interaction is rather complicated, e.g. due to the existence of interfering resonances.

The lifetime of formed resonances is stochastically chosen according to an exponential decay law. The average lifetime (without collisions) is given from the inverse decay width. The angular distributions in decays of formed resonances are certainly an area in which more work is needed. All transport models for  $AA$  collisions so far had ignored this problem, which is already present in the ‘prototype’ reaction  $\pi N \rightarrow \Delta(1232) \rightarrow \pi N$ , by decaying the resonances isotropically. While the problem can be easily solved for isolated resonances, it becomes more involved for overlapping resonances. The different partial waves should be summed coherently which would generate a diffraction-type peak at small scattering angles. As a first step isotropic resonance decay is supplemented in RQMD by a second component, a Gaussian  $p_t$  distribution. This ensures that the average  $p_t$  which is generated does not exceed the standard value of 400 MeV which is usually assigned to a produced quark pair in soft production processes at high energy.

---

<sup>6</sup> Some of the resonance parameters have been changed slightly as compared to the values given in [33], because they were refitted together with the modified continuum component to  $\pi N$  data.

## 3.2 Transition from $s$ channel resonances to Reggeon exchange

The formation of discrete  $s$  channel resonances, which represents the low energy component of quark-antiquark annihilation in  $hh$  interactions, has just been described in some detail. Such a description is expected to break down in the intermediate CMS energy region  $s = 4 - 16 \text{ GeV}^2$ . Resonance level densities are getting too high and resonance widths too large that a formulation in terms of discrete resonance excitations could be meaningful. Furthermore, due to these difficulties the empirical information about discrete states gets poorer with increasing invariant resonance mass. On the other side, Regge theory is spectacularly successful in this energy region. I do not discuss here the speculation that an infinite tower of  $s$  channel resonances could effectively generate the same interaction as  $t$  channel Reggeon exchange (see e.g. the Veneziano model [63]).

The main emphasis is put in this subsection on a discussion of  $B=1$  channels. The continuum component in  $MB$  reactions is of utmost importance for nucleus-nucleus collisions due to preequilibrium processes [13], while it is suppressed kinematically in  $MM$  collisions. For instance, here the processes are above threshold for  $s\bar{s}$  creation. There is one more reason to model carefully  $MB$  interactions in this energy region. Strange (anti-)baryons are a very promising signature of collectivity in ultrarelativistic nucleus-nucleus reactions. After they are produced in an  $AA$  collision, they have to propagate eventually through a cloud of nonstrange mesons [14]. The strength of transition rates like  $\Lambda\rho \leftrightarrow \bar{K}N$  or  $\Xi K \leftrightarrow \bar{K}Y$  is determined by the probability of moving the  $s$  quark from the baryon to the meson side (and vice versa).

The total strength and the energy dependence of the Reggeon exchange component follow from the ansatz which was introduced above:

$$\begin{aligned} \sigma_{Regge}(s) &= (\sigma_{tot}(s) - \sigma_{BW}(s) - \Delta\sigma(s)) && \text{for } s \leq s_0 \\ &= (\sigma_{tot}(s) - \sigma_{BW}(s) - \Delta\sigma(s)) \cdot \sqrt{s_0/s} && s > s_0 \end{aligned} \quad (15)$$

for  $\pi N$ ,  $\bar{K}N$  and  $\pi\Xi$  interactions. Eq.(15) is applied for  $MB$  states of good flavor quantum numbers (isospin, hypercharge). Interference effects of amplitudes in different states are neglected. The  $\sqrt{s_0}$  parameter is set to 1.8 GeV in the  $N^*$ , 2 GeV in the  $\Delta^*$  and  $Y^*$ , and 2.15 GeV in the  $\Xi^*$  channel.  $\Delta\sigma(s)$  is given from the elastic background cross sections for  $\pi N$  or the sum of the tabelized cross sections  $\bar{K}N \rightarrow \bar{K}N$ ,  $\pi\Lambda$ ,  $\pi\Sigma$  for  $\bar{K}N$  collisions. Ac-

cording to eq. (15) the contribution of the Breit-Wigner resonances in the  $N^*/\Delta^*/\Xi$  channels have to be subtracted to get the total ‘Reggeon exchange component’. Note that the tails of the  $N^*$  and  $\Delta^*$  resonances above  $s_0$  are calculated from eq. (13) with the  $b(s)$  values ‘frozen’ to the value of  $b$  at  $s=s_0$ .

No experimental data are available for the total  $\Xi\pi$  cross section. Its value above  $s_0$  is taken from the additive quark model (AQM). Lack of experimental information is the reason that fewer  $\Xi^*$  resonances are included in the Breit-Wigner sum of eq. (13) than in other channels. This is ‘corrected’ in eq. (15) by multiplying the constant AQM value by  $\sqrt{s_0/s}$  for  $s$  smaller than  $s_0$  down to the  $\Xi^*(1530)$  resonance, if the Breit-Wigner sum gives a smaller value for the cross section than this parametrization.

There is no Reggeon exchange component in the  $N^*$  and  $\Delta^*$  channel for energies below  $s = s_0$ . (The annihilation cross section is filled up by  $s$  channel resonance formation according to eq. (13).) In the  $\Lambda^*$  and  $\Sigma^*$  channels the Reggeon exchange component is present down to lower energies, because the difference of the total cross section to the sum of the tabelized cross sections becomes nonzero, even below invariant mass of 2 GeV/c<sup>2</sup>.

The total Regge exchange component as given by eq. (15) can be subdivided into single Reggeon exchange ( $2 \rightarrow 2$ ) and into multi-Reggeon exchange ( $2 \rightarrow 3, \dots$ ) diagrams. Multi-Reggeon exchange diagrams with  $n > 2$ -body final state may become important to account for some fraction of multiparticle production at higher energies. However, such processes are suppressed in the hadronic rescattering stage of  $AA$  collisions [13]. Their presence would be indicated by an additional component to the produced particle yields nonlinearly increasing with the number of participant nucleons for which there is also no hint from experimental data. Before the relative weights for these two classes of processes in RQMD are discussed, it is useful to describe how a particular 2-body final state in a reaction of the type  $M_i B_i \rightarrow M_o B_o$  is selected out of the sample of all possible states.

The exclusive cross sections of the Regge exchange component  $2 \rightarrow 2$  have been given the following functional form:

$$\sigma(M_i B_i \rightarrow M_o B_o) = \frac{1}{p^2(2S_{M_i} + 1)(2S_{B_i} + 1)} \sum_I a_I(s). \quad (16)$$

$$\left\{ |C_{MB,I}|^2 \left(1 - \exp\left(-\left(p_{MB}/\sigma\right)^2\right)\right) \left((2S_M + 1)(2S_B + 1)\right) r(R) \right\}_{in}$$



$$\cdot \left\{ \dots \right\}_{out} \left( 1 + pp'/p_R^2 \right)^{-\Delta\alpha_R} .$$

Eq. (16) contains several factors – in their ordering from the left to the right – related to incoming flux and spin averaging, absolute normalization ( $a_I(s)$ ), isospin projection (Clebsch-Gordon-coefficients squared), threshold phase space factor, internal spin degrees of freedom, suppression parameter  $r(R)$  of strangeness creation or quark exchange between  $M$  and  $B$ , and a suppression for exchange of Reggeon  $R$  as determined by the intercept of the corresponding Regge trajectory  $\alpha_R$ . If the absolute normalization is ignored for the moment, the relative probability of some final state is determined rather simply. Up to some statistical factors which express the ‘matching’ of the isospins and the available spin degrees of freedom there are only three factors which contain dynamics: the phase space factor, the strangeness parameter  $r(R)$ , and the Regge factor. Since the Regge factor tends to 1 at low relative CMS momenta  $p$  and  $p'$ , the approach assumes kind of ‘universal’ (or average) coupling of a meson-baryon 2-body state to the intermediate system with baryonic quantum numbers. The phase space factor cuts down on the production probability near threshold, but then also goes quickly to 1. Its functional form is motivated by the available phase space for Schwinger type  $p_t$  creation in flux-tube decays which is Gaussian distributed, with width  $\sigma=400\text{MeV}$ . The parameter  $r(R)$  is assigned a value different from 1 only to account for  $s\bar{s}$  suppression (0.3 in a connected and 0.09 in a disconnected quark-line diagram) and to suppress exchange of quarks between  $M$  and  $B$  in some processes (0.5 for exchange of baryon number or strangeness). The first parameter is the usual strangeness suppression which is characteristic for soft particle production. The last parameter value reflects the immobility of the heavier strange quark and of the leading spectator diquark. The model presented here is very similar in its spirit to Vandermeulen’s statistical approach [64], and Mundigl, Vicente Vacas and Weise’s doorway model [65], both for meson production in low energy  $\bar{p}p$  annihilation. This is not really a surprise, because the common denominator is the overwhelmingly large number of open states which precludes any kind of detailed dynamical treatment.

Some additional strangeness suppression is ‘hidden’ in the Regge factor which is smaller for strange Reggeon exchange. It is a general observation that the strangeness suppression in nonexotic  $hh \rightarrow hh$  interactions is some-

what stronger – in addition to phase space suppression – than ‘asymptotically’ in soft hadronic physics ( $P(s)/P(u)$  is  $\approx 0.3$  for multiparticle production). See e.g. the suppression parameters for kaon channels in  $\bar{p}p$  annihilation [64, 65] which are needed to fit the experimental data. A stronger  $s\bar{s}$  suppression is expected from microscopic calculations which give a larger suppression for heavy mass quarks if a color flux-tube has a small length or breaks very early [53]. However, it cannot be ruled out that part of the stronger suppression effect comes from the neglect of quark exchange diagrams. Their inclusion – in reactions without strange quark in the initial state – favors nonstrange final states. It has been found for  $MB$  interactions that an average strangeness suppression parameter of 0.2 can reasonably well describe total strangeness creation in  $\pi N$  reactions [33]. Therefore not too much freedom is left for a pure quark exchange component in such reactions.

The Reggeon exchange suppression factor contains the momentum  $p_R$  as a scale at which Reggeon exchange becomes important. Thus the parameter choice reflects the interpolation from the  $s$  channel resonance region to the high energy Regge approach.  $\Delta\alpha_R$  is defined as

$$\Delta\alpha_R := 2 - 2\alpha_R - \alpha_0 \quad . \quad (17)$$

For each  $M_i B_i \rightarrow M_o B_o$  reaction only a single Regge trajectory is taken into account, the one with largest intercept. The vertices which are used in the RQMD calculations are presented in tables 1 and 2, together with the parameters for the Reggeon intercepts.

The multi-Reggeon component is represented in the model by a  $hh$  annihilation into a color string which decays into more than two hadrons (resonances) according to the standard string fragmentation scheme. In principle, the probability whether a 2-body final state ( $2 \rightarrow 2$  process) or an  $n$ -body final state ( $n > 2$ ) is chosen in a Reggeon exchange process is determined by the normalization factors  $a_I(s)$  in eq. (16). However,  $a_I(s)$  is not specified explicitly in RQMD. Instead, the correct Regge behaviour for  $2 \rightarrow 2$  processes at large energies provides an implicit normalization of the total  $2 \rightarrow 2$  Reggeon-exchange cross section. Regge theory requires all  $2 \rightarrow 2$  cross sections to behave (approximately) as

$$\sim s^{2\alpha_R - 2}$$

at large energies. With the parameter choice  $\alpha_0=1$  the cross sections of eq. (16) show this behaviour under the assumption that  $a_I(s)$  approaches a

constant value at high energies.

The correct asymptotic behaviour for 2→2 transitions is realized in the following way. For invariant masses of the colliding  $M_i B_i$  pair below some value  $\sqrt{s_1}=2.8$  GeV (plus 0.15 GeV for each s quark in the  $B^*$  state due to flavor symmetry breaking) it is assumed that all final states are 2-body. Above  $s_1$  the 2-body final state is suppressed by an additional power 1/2

$$\sigma_{Regge}(2 \rightarrow 2) \leq \sigma_{Regge}(s) \cdot \sqrt{s_1/s} \quad , \quad (18)$$

and the appearing gap to the total Reggeon-exchange cross section is filled up by choosing an  $N>2$ -body final state. The  $\leq$  sign in eq. (18) is to be understood in the sense that  $\sigma_{Regge}(2 \rightarrow 2)$  is assigned at first a value which is equal to the right hand side of eq. (18). The normalization according to eqs. (15) and (18) would give asymptotically a  $1/s$  dependence for  $\sigma_{Regge}(2 \rightarrow 2)$  if the equal sign in eq. (18) would hold. This is actually the correct energy dependence if Reggeons of the  $\rho$  trajectory with the largest intercept are exchanged (the  $\alpha_\rho \simeq 0.5$ ). On the other side, cross sections for other transitions  $M_i B_i \rightarrow M_o B_o$  may drop faster with energy due to a smaller intercept parameter  $\alpha_R$  of the exchanged Reggeon. In order to avoid that cross sections characterized by a comparably larger intercept  $\alpha_R$  simply blow up due to the normalization condition in eq. (18), a fraction of the total 2→2 Reggeon-exchange cross section goes actually into many-body final states. This will be explained in the following.

After the decision to choose a 2-body state has been made in RQMD, a particular state has to be selected, respecting its relative weight according to eq. (16). This is realized in a Monte Carlo-type fashion using the rejection method. After some randomly chosen out-state has passed all other acceptance tests, the Reggeon factor

$$p_{Regge}(s) = \left(1 + pp'/p_R^2\right)^{-\Delta\alpha_R} \quad (19)$$

is taken as a probability for final acceptance of the 2-body state. Below  $s_1$ , Monte Carlo type rejection of a 2-body channel is followed by choosing another 2-body state until at last an out-state passes all acceptance tests successfully. Above  $s_1$ , the acceptance probability is again given by  $p_{Regge}(s)$ . However, the probability to examine another 2-body state is frozen at the value  $1-p_{Regge}(s_1)$ . As a third possibility, an  $N>2$ -body final state may be chosen, with probability

$$\text{probability}(N > 2) = p_{Regge}(s_1) - p_{Regge}(s) \quad \text{for } s > s_1 \quad .$$

This prescription guarantees the continuity of all cross sections across  $s_1$  and the correct energy dependence of all  $2 \rightarrow 2$  cross sections asymptotically.

Which hadrons are included in the in- and out-states of eq. (16)? All nonstrange baryon resonances with a pole mass below  $2 \text{ GeV}/c^2$  whose existence is established by the Particle Data Group can be produced. All baryon multiplets with these  $N^*$  and  $\Delta^*$  states have been completed by including strange baryon resonances either according to the data tables, flavor  $SU_3$  relations or by applying a simple formula for resonance mass ( $m = m(N^*/\Delta^*) + n_s \cdot 150 \text{ MeV}$ ) and width ( $\Gamma_R = d_R \Gamma(N^*/\Delta^*)$  with  $d_R$  equal 0.85 for  $\Sigma^*$ , 0.62 for  $\Xi^*$  and 0.45 for  $\Omega^*$ ). Thus an unwanted flavor  $SU_3$  breaking due to the poorer experimental knowledge of resonances in the strange resonance sector is avoided. In a second step the formed resonance states decay subsequently. The branching ratios of those resonances whose properties are not taken from the data tables or flavor  $SU_3$  relations have to be specified. They are determined similarly as given for the intermediate doorway state in eq. (16), however, without Reggeon factor:

$$\Gamma(B^* \rightarrow MB) \sim \tag{20}$$

$$|C_{MB,I}|^2 \left(1 - \exp\left(-\left(p_{MB}/\sigma\right)^2\right)\right) \left((2S_M + 1)(2S_B + 1)\right) r(B^*) \quad .$$

Here the parameter  $r(B^*)$  is related to strangeness again. Its value is set to 0.2 if  $s\bar{s}$  is created in the decay (1 otherwise). Of course, strangeness creation in a second step is much more improbable than in the first stage of interaction given by eq. (16).

With the combined model of  $s$  channel resonance formation and  $t$  channel Reggeon exchange one can describe reasonably well on the order of 60 measured exclusive meson-baryon reactions ( $\pi N$  and  $\bar{K}N$ ), including their energy dependence. Usually the results agree with exclusive 2 and 3-body data better than within a factor of two. Inclusive yields, especially of strange hadrons (kaons, hyperons, etc.), are described even much better (within 10 percent). The constructed model does not aim for a ‘perfect’ fit to experimental data. Instead, the intention was to introduce only a minimum number of parameters whose values have some physical meaning like strangeness suppression, the scale which separates the resonance from the Regge region and so on. Therefore the model can be meaningfully extrapolated to ingoing  $hh$  combinations with experimentally unexplored properties of their interactions. No new parameters have to be introduced if the  $\pi$  or  $\bar{K}$  and the nucleon are replaced by other meson-baryon combinations, in particular resonances. Their

low and medium-energy interaction are completely specified by the same model, essentially given by eqs. (13) and (16). The interactions fulfill the property of *detailed balance*. Detailed balance follows from the time reversal invariance of strong interactions. A cross section  $\sigma_{io}$  for a  $M_i B_i \rightarrow M_o B_o$  transition is related to the cross section in the reverse direction by

$$\sigma_{oi} = \frac{p^2(2S_{M_i} + 1)(2S_{B_i} + 1)}{p'^2(2S_{M_o} + 1)(2S_{B_o} + 1)} \sigma_{io} \quad . \quad (21)$$

Thus the model avoids the pitfalls of equating cross sections with ingoing resonances to groundstate hadrons as used in early RQMD calculations [3] and in other transport models [20, 28].

After the discussion about the quark annihilation processes in the continuum has focused so far on  $B=1$  channels, I would like to discuss shortly its role in channels with total baryon number zero. Such reactions can be either  $\overline{B}B$  annihilations or  $MM$  interactions. The  $MM$  annihilation into a continuum is constructed very similarly to the approach outlined above for  $MB$  interactions. The continuum annihilation starts to open up at  $s_0 = ((1.6 + n_s \cdot 0.15) \text{ GeV})^2$ , because the Breit-Wigner resonance tails decay faster than  $s^{-1/2}$  which again is the assumed energy dependence of the total annihilation cross section. Note that the coupling between 2-body in- and out-states is not reggeized yet. Instead, the couplings are constants with strangeness annihilation and creation suppressed by the factor 0.2 as in [33, 65]. A parametrization of the  $\overline{p}p$  annihilation cross section is used which was fitted to experimental data [66]. The construction of the other  $\overline{B}B$  absorption cross sections is described in [13]. In principle, one should put the same effort into a detailed description of the out-states as discussed for  $MB$  interactions. However, the choice of the outgoing states in the continuum region is of minor importance for the reaction dynamics of heavy ion collisions.  $MM$  collisions around an invariant mass of 2 GeV/ $c^2$  are rather rare in  $AA$  collisions [13], because too much internal kinetic energy is required. Clearly  $\overline{B}B$  collisions are not kinematically suppressed in this invariant mass region. Therefore the final  $\overline{B}$  yield is very sensitive to the annihilation strength. However, it matters only whether an antibaryon survives in baryonic matter or not. The specific choice for the particle production model in  $\overline{B}B$  annihilations has not much influence on the meson dynamics itself. Note that the typical  $\overline{B}/M$  ratio in central  $AA$  reactions at 200 AGeV is on the one percent level only. So far the RQMD procedure for the choice of the outgoing states in the  $B = 0$  system is to form a mesonic string which decays according to

the standard rules of string fragmentation. In addition, it is enforced that  $G$  parity is conserved in nonstrange meson transitions by rejecting out-states with wrong  $G$  parity.

Particle production at energies in the ‘continuum’ region, i.e. beyond the regime of identified resonance decays, can be naturally viewed as a tunneling process of quark pairs leading to subsequent breaking of a color flux-tube [51]. Thus the annihilation processes in the continuum are translated in RQMD into the language of (Yo-Yo type) string decay. This determines the space-time structure, most importantly the formation points of outgoing hadronic states.

### 3.3 Meson exchange processes in the $t$ channel

Here I am going to discuss the component in RQMD which describes  $t$  channel exchange driven processes in  $MM$  interactions with two mesons or resonances in the final state. Meson-exchange processes in  $MM$  interactions are generated by a flavor  $SU_3$  symmetric Lagrangian which couples a vector meson to two pseudoscalar mesons.<sup>7</sup>

The empirical knowledge about meson-meson interactions is rather poor due to the inherent difficulty to prepare a mesonic ‘target’. Only  $\pi\pi$  and  $\pi K$  interactions are well explored. It has been outlined above that formation of the  $\rho$  and  $K^*$  resonance are dominating the interactions in these channels. The decay of the vector meson resonances into two pseudoscalars is approximately described by a flavor  $SU_3$  symmetric interaction term in the Lagrangian

$$L_{\text{int}} = -(i/2)G_V \text{Tr}([\hat{P}, \partial_\mu \hat{P}]\hat{V}^\mu) = 2G_V f_{ijk} P_i \partial_\mu P_j V_k^\mu \quad . \quad (22)$$

$\hat{P}$  and  $\hat{V}$  denote the pseudoscalar and vector meson matrix [71]. Flavor symmetry is broken only by the mass differences between mesons within the multiplets.

In addition to vector meson decay, the  $SU_3$  invariant Lagrangian in eq. 22 generates transition rates for reactions  $PP \rightarrow PP$ ,  $PV \rightarrow PV$  and  $PP \leftrightarrow$

---

<sup>7</sup> In addition, RQMD includes parametrizations of cross sections involving nucleons and the  $\Delta(1232)$  resonance which were calculated using the One-pion-exchange model (OPE) [67, 68], e.g.  $NN \leftrightarrow N\Delta$ , or OPE-inspired parametrizations of some measured flavor creating processes like  $NN \rightarrow \Delta(1232)YK$  [69, 70]. These processes are of not much importance in 200A GeV collisions, the topic of this paper.

$VV$  by exchanging a meson in the  $t$  channel.  $G_V$  is fitted to the  $\rho$  decay width and set to 3.02. All relativistic Born diagrams for flavor changing processes and for all important exotic channels (which have no other interactions at low energy) have been calculated and implemented in RQMD. The interaction vertices are supplemented with monopole form factors

$$f(t) = \frac{\Lambda^2 - m^2}{\Lambda^2 - t} \quad , \quad (23)$$

which express the finite size of the interacting mesons. The wrong energy dependence in reactions with vector meson exchange is ‘cured’ by multiplying each PPV-vertex with  $(s/s_0)^{(\alpha_0-1)/2}$  for  $s > s_0$  ( $\sqrt{s_0}=1\text{GeV}+m_1+m_2$ ).  $SU_3$  invariant values for the cutoff-parameter  $\Lambda$  are chosen,  $\Lambda = 3.0 \text{ GeV}^2$  ( $1.5 \text{ GeV}^2$ ) for attraction (repulsion) in the  $s$  wave. The calculated interactions give remarkably good agreement with the measured phase shifts in  $\pi\pi$  and  $\pi K$  interactions [58],[72]-[74]. As an example the  $s$  wave phaseshift is shown for  $\pi\pi$  scattering with  $I=0$  and  $I=2$  (cf. fig. 6). Note that the  $I=2$  channel is exotic, while the  $I=0$  channel contains additional contributions from  $s$  channel resonances, in particular the  $f_0(975)$  and the  $f_0(1400)$ . A completely unitarizing scheme – eq. (11) below  $K\bar{K}$  threshold and its generalization, the Davies-Baranger formalism, above threshold – has been applied to calculate the combined effect of  $t$  channel background and  $s$  channel resonances. The real-valued matrix elements for one-meson-exchange have been identified with the  $K$  matrix which has been decomposed into their components from different partial waves. The background  $S$  matrix for partial wave  $l$  is constructed from the  $K$  matrix via:

$$S_{bg}^l = (1 + iK^l)(1 - iK^l)^{-1} \quad . \quad (24)$$

While a standard parametrization is used for the  $f_0(1400)$  decay width, the  $K\bar{K}$  molecule picture is employed for the  $f_0(975)$  [75]. Furthermore, the  $f_0(975)$  decay width into  $K\bar{K}$  is analytically continued below threshold like in Ref. [76] in order to generate the sharp cusp observable in the scalar-isoscalar phase shift just below  $\sqrt{s}=1 \text{ GeV}$ .

## 4 Flavor production in central Pb(160AGeV) on Pb collisions

The two basic building blocks of interactions in RQMD – color ropes and hadronic rescattering – have been presented in the preceding sections. In this section the consequences of these collective interactions for the flavor dynamics in the most central collisions of two lead nuclei at a beam energy of 160AGeV will be discussed. The impact parameters for the calculated Pb(160AGeV) on Pb collisions have been selected between 0 and 1 fm, rather central collisions. The calculations with the RQMD computer code have been done in different modes, the default mode and two alternative modes. The first alternative mode is defined by switching off all collective interactions, no rescattering and no rope formation (‘NN mode’). The second non-default mode is without rescattering but rope formation included.

### 4.1 Particle multiplicities

The results of the different RQMD calculations for the final hadron yields are presented in table 3. All members of the basic pseudoscalar meson nonet and (anti-)baryon octet have been kept stable here with the exception of the  $\eta'$  which decays already during the dynamical evolution generated by RQMD. Some extreme scenarios are a scaling of the totally produced hadron yield with either the number of participants or the number of binary collisions. These scenarios lead to an  $A^\alpha$  dependence of the produced particle multiplicities with  $\alpha$  values of 1 and 4/3. One would get the  $\alpha$ -value 4/3 from RQMD in the ‘NN mode’ by neglecting finite-energy effects. In this case the final particle yield would simply scale with the number of binary collisions, because in each collisions new strings can be created and each string decay gives asymptotically a constant rapidity density. The number of created quark pairs in the ‘NN mode’ of RQMD is 3061 which gives more than 7.2 created hadrons per participating nucleon. This can be compared to the corresponding numbers in elementary  $pp$  collisions which is 4.9 (at the slightly higher beam energy of 200AGeV). In terms of an  $A^\alpha$  parametrization this means an  $\alpha$ -value of 1.07 by comparing Pb+Pb and  $pp$  reactions. This value is still far away from the ‘upper limit’ 4/3. Obviously the finite-energy effects – finite string masses and mutual deceleration of projectile and target – change the naive estimate considerably.



How do the production rates of quark pairs change if rope formation is taken into account in Pb(160A GeV) on Pb collisions? The formation of coherent chromoelectric fields which fill the space between the receding color charges sets different initial conditions for particle creation than the incoherent superposition of elementary strings. The effect of ropes on the conversion rate of field energy into  $q\bar{q}$  pairs, the resulting rope lifetime and particle multiplicities have been discussed already in the literature [4, 55]. Neglecting partially or completely the screening effect of already produced charges and employing various approximations, in particular boost invariance, simple relations for these variables as a function of the rope field strength have been derived. The authors of Ref. [4] derive a relation valid in their model

$$F(K)/F(1) \approx 2.12 \quad K \rightarrow \infty \quad , \quad (25)$$

with  $F$  the meson multiplicity and its argument the so-called foldness. The foldness  $K$  is defined by the number of (anti-)triplet charges which screen a rope field completely.  $K=p+q$  for a rope whose source is a color  $SU_3$  charge in the  $(p,q)$  representation. Eq. (25) implies a strong suppression of particle production  $\sim 1/N$  compared to production from  $N$  independent strings. Note that random charging without any constraint leads to the average  $K$  value

$$\langle K \rangle \approx \sqrt{N} \quad .$$

The multiplicities from rope fragmentation in RQMD cannot be calculated analytically, but show similarly a trend that particle production is strongly dampened with increasing rope charge. The assumption that each hadronizing string breaks just once seems more appropriate for an estimate of the rope effect at 160A GeV on multiplicities than the opposite extreme of an infinite number of break points which is a consequence of assumed boost invariance. Under this assumption the number of created quark pairs is depleted if ropes are formed, because the minimum number of quark pairs to screen the original field is smaller ( $\sqrt{N}$  versus  $N$ ). Thus the total number of quark pairs including the quarks of the source charge is given simply as  $2N$  from  $N$  string decays,  $\sqrt{N}+N$  from rope fragmentation.

Neglecting finite-energy effects grossly overestimates the influence which rope formation can have on the whole dynamical evolution of the system. After the hadrons which contain ingoing constituent quarks have been subtracted from the average number of primary hadrons in elementary  $hh$  collisions at 160 GeV is around 2 per collision partner. Subsequent collisions in

a nuclear target produce effectively even fewer hadrons per collision which come from smaller strings or from excited resonance decays.

The surface and the finite thickness of the ingoing nuclei play a nonnegligible role as well for rope formation. The Lorentz contracted lead diameter in the C.M. frame is approximately 1.4 fm. The corresponding passage time for the collision partner has therefore a value which is larger than the hadronization scale (1 fm/c). Strings or ropes which were formed early in the collision may have already hadronized before the projectile has completed its passage through the target. All these effects tend to suppress the importance of rope formation and favor the other sources of secondaries, elementary strings and resonances.

The RQMD approach to rope formation and hadronization is superior to schematic calculations, also because it respects the simple constraints arising from nuclear geometry and finite beam energy. The yield of produced secondaries decreases from 3006 to 2571 in the calculated central Pb on Pb collisions by allowing string fusion into ropes. This 15%-effect on the total multiplicity from rope formation is tiny as compared to the suppression effect implied by eq. (25). It will be interesting to study the energy dependence of the multiplicities in case of rope formation. The dampening of particle production due to formation of strong chromoelectric fields should become much more pronounced at collider energies.

Inclusion of hadronic rescattering leaves the total produced particle multiplicities practically unchanged (2512 in comparison to 2571 without rescattering). These values correspond to an  $\alpha$ -value of 1.04 which is even closer to 1 yet than in the ‘NN mode’ of RQMD. The reason is that particle number conserving processes – in RQMD  $2 \rightarrow 2$  – dominate the rescattering stage. Particle conservation in the expansion stage of  $AA$  collisions has been conjectured by other authors earlier based on general grounds (kinetic equilibration together with  $G$  parity conservation which forbids to change the pion number by one unit in collisions of nonstrange mesons) [77] and is confirmed by the microscopic transport calculations. The small decrease of the particle multiplicity due to rescattering is connected with the strangeness enhancement (see below) and the related smaller feed-down of the lightest hadronic degree of freedom, the pions. One should keep in mind that the strange hadrons,  $\Lambda$ ,  $K_S$ , etc. are considered stable here.

## 4.2 Rapidity distributions

Here I shall focus on the shapes of the rapidity distributions for different particle species. The rapidity distributions for negatively charged hadrons calculated in the different RQMD modes are displayed in fig. 7. It is clearly visible that the change in produced particle multiplicities is concentrated in the central region. The collective effects leave practically no tracks in the fragmentation region of projectile and target ( $|y_{CMS}| > 2$ ). At these rapidities the three rapidity distributions – from the ‘NN mode’, with ropes and with additional rescattering fall on top of each other. This can be understood from the discussion in section 2.2. The rope fields influence mainly the particle multiplicities at rapidities which are covered by many strings. Also the small absorption effect which rescattering has on the particle multiplicities is concentrated around midrapidity. On the left hand side of fig. 7 the net proton ( $p-\bar{p}$ ) rapidity distribution is shown for comparison. The  $p-\bar{p}$  rapidity distributions are remarkably similar in the three RQMD modes. Rescattering makes the final net baryon distribution only slightly narrower. The small effect of hadronic rescattering on the baryon stopping in the present RQMD calculations differs markedly from results in the string model QGSM (without string fusion but rescattering included) [78]. The effect in the calculation presented here is also somewhat smaller than in early RQMD studies [80]. The difference is mainly caused by the more realistic angular distribution in baryon resonance decays (see section 3.1 for a discussion). Isotropic decay as employed in Ref. [80] tends to shift baryons rather rapidly into the central region. One can see from fig. 7 that the  $p-\bar{p}$  rapidity distribution is significantly broader than the produced particle distribution. However, the baryon stopping mechanism in RQMD is much more pronounced than in other approaches [41, 79]. In RQMD it shows no minimum at midrapidity but a plateau in the central region.

The comparison of the rapidity distributions of net protons and negatives in fig. 7 demonstrates that the single fireball picture is inconsistent with the calculated rapidity distributions, like in the smaller S+A reactions [13]. The primordial nucleon rapidity density would have a width between 0.44 and 0.52 units at freeze-out temperature between 140 and 200 MeV. The heavier a particle, the narrower is its rapidity distribution in a thermal fireball. The reverse ordering found from RQMD is indicative for the presence of longitudinal flow in the system. One could imagine different mechanisms driving the

longitudinal flow, internal pressure (as in Landau scenario) or a transparency effect (as in Bjorken scenario). RQMD in which the secondaries are initially created by the boost-invariant decay of a longitudinally stretched tube is constructed very similarly to a Bjorken-type approach. Some differences arise from finite-energy effects which are clearly visible from fig. 7. There is no plateau in the produced particle rapidity distribution at all. Furthermore, the Bjorken ansatz of identifying space-time and momentum-space rapidity is ‘softened’ in string models resulting in a finite width of the local rapidity distribution [33]. The calculated rapidity distribution of negatively charged hadrons is narrower in central Pb on Pb than in S(200AGeV) on S collisions. The width of the distribution is 1.6 units of rapidity versus 1.9 which makes a difference of 8% if they are normalized to the initial rapidity gap between projectile and target. The narrowing arises in the model from the stronger attenuation of the ingoing nuclear constituents in the heavy system. It is interesting to note that Landau-type hydrodynamics with all matter initially at rest would show the opposite effect. Fig. 8 displays the calculated rapidity distributions of strange baryons and mesons. The distributions of strange baryons are markedly narrower than the proton density, 1.7 versus 2.1. This cannot be attributed to the mass differences which results only in small width differences in a thermal picture ( $< 0.05$ ). Taking longitudinal flow into account does not explain this effect either. In RQMD it reflects differences in the production dynamics. The probability that a baryon carries finally a strange quark is correlated with its rapidity. Baryons at central rapidity have suffered simply more collisions, initially with nucleons from the other nucleus, later on with secondaries. Spatial inhomogeneity of the flavor composition is no real surprise, even in collision of truly heavy ions. On the other side, parametrizations of ‘hydrodynamical flow’ under the homogeneity assumption have been quite popular for studies of light ion reactions [81, 82]. One can take the RQMD calculations presented here as an indication that results in such simple models have to be taken with some grain of salt.

The final antikaon and kaon distributions have a slightly smaller width (1.3-1.4) than the hyperons as a result of the generated longitudinal flow. In contrast, the antibaryon rapidity densities have much smaller widths (1.1-1.2) than mesons and baryons as can be learnt from the results presented in fig. 9. Again, this effect is incompatible with a homogeneous thermal fireball – with or without longitudinal flow – and reflects different production mechanisms in the model. Since antibaryons are mostly produced in rope fragmentation

(see below), they are primarily formed in position and rapidity space where many strings overlap. Baryon pairs emerge only from the regions of highest energy density. In contrast, due to smaller production threshold  $s\bar{s}$  pairs are created also in the diluter regions as well. It had been already noted by the experimentalists in the presentation of first data for S(200AGeV) on S collisions that the different shapes of  $\Lambda$  and  $\bar{\Lambda}$   $dN/dy$  distributions provide evidence for differences in the production mechanisms [83]. The systematics of measured strangeness and antibaryon production in S on A collisions at beam energy of 200AGeV [84] can be exploited to understand better the dependence on initial baryon and energy density. The latter variables are related to the final baryon and meson rapidity densities. It was argued in [13] that the narrow antibaryon distributions in S+A reactions <sup>8</sup> arise as a convolution of two effects, string or equivalently energy density, which is the determining factor in the model for the achievable rope field strength, and the smoothly increasing baryon density (in position and momentum space) towards the target rapidity region. In contrast, in central Pb on Pb reactions the antibaryon rapidity densities get slightly broadened due to absorption, because the rather flat net baryon density for Pb on Pb is centered around midrapidity.

### 4.3 Strangeness enhancement

How large is the fraction of created strange quarks relatively to the light flavors from RQMD? The fraction of created  $s\bar{s}$  pairs normalized to the average of  $u\bar{u}$  and  $d\bar{d}$  pairs

$$R_s = \frac{2N(s\bar{s})}{N(u\bar{u}) + N(d\bar{d})}$$

turns out as 11.3% in the ‘NN mode’ which should be compared to 10% in  $pp$  collisions at 200GeV, a small increase. <sup>9</sup> The rate of produced kaons remains practically unchanged in the ‘NN mode’ if they are normalized to the pion yield. For instance, the  $K^-/\pi$  ratio is 6 percent (with isospin averaged pion yield) while it is 5.6 % in  $pp$  collisions. Several competing effects may give rise to small deviations from the  $pp$  result. Because of energy degradation the average string masses are lower in multiple collisions of a projectile hadron

---

<sup>8</sup> Note that the  $\bar{p}$  distributions for the calculated reactions with O and S projectiles in fig. 5 of Ref. [13] are scaled by a factor of 10 (not 20 as indicated in the figure).

<sup>9</sup> It is neglected here that  $\eta$  and  $\eta'$  meson carry some amount of hidden strangeness.

impinging on a nuclear target. This effect is unfavorable for strange particle production. On the other side, the ingoing flavor has to be used up if only one string is excited in course of a nucleon collision. If several strings are attached to an ingoing interacting constituent quark, all of the additional strings have color charges from the sea, possibly an  $s$ -quark, at their end points. Furthermore, multi-step processes of the type  $B \rightarrow B^* \rightarrow B^{**}$  which are most relevant near particle production threshold may still play a small role even at a beam energy of 160 AGeV.

The strange baryon rate normalized to the total baryon number increases considerably already in the ‘NN mode’. The ratio of  $\Lambda/B$  including all feed-down contributions is 0.05 in  $pp$  collisions from RQMD which is in accordance with experimental data [85]. It increases by nearly a factor of 2 to a value of 0.09 in central Pb on Pb reactions. This effect can be understood rather simply from the multiple collision effect on baryons (see the diagrams in fig. 2). While only 1 or 2 of the original valence quarks are replaced in elementary  $NN$  collisions, the large majority of valence quarks are being replaced in the outgoing baryon states by quarks from the sea in Pb on Pb collisions at small impact parameters. Thus the probability increases with the number of collisions which a baryon undergoes that it will carry a single or even multiple units of strangeness after the interaction. A similar effect is observed in the VENUS approach to  $AA$  collisions which includes the mechanism of ‘double-string’ formation [24].

A strong strangeness enrichment compared to the ‘NN mode’ and the calculated values for  $pp$  collisions is expected by including the collective interactions into the calculations. The suppression of heavy quark production in strong chromoelectric fields is weakened. The different barrier penetration factors for virtual quark tunneling are approaching the same values. Rescattering processes tend to enrich strangeness in nuclear collisions, because – starting under conditions in which strangeness is undersaturated – nonstrange quark pairs are preferentially annihilated in resonance and string formation processes and sometimes replaced by a strange quark pair in the decay. Associated production plays the most important role for strangeness enhancement in the hadronic resonance gas. The difference between a  $\Lambda$  baryon and nucleon mass is just 178 MeV, but twice this value between anti-kaon and pion mass. Furthermore, the preequilibrium contribution to the secondary interactions is stronger in the meson-baryon than the meson-meson sector [13]. This is qualitatively easily understood, because the baryon

rapidity distribution is broader than the meson distribution. This holds also locally which is responsible for the hard tail in the collision spectrum of baryons. Transport calculations with the RQMD model show good agreement with available data for reactions with light ion projectiles which are sensitive to this production mechanism (net- $\Lambda$  rates,  $K^+/K^-$  enhancement) [11, 13].

Most of the strangeness is carried in the final state by (anti-)kaons which makes their yield normalized to the total produced particle multiplicity to a signature for the strength of collective effects in AA collisions. It has been discussed already some time ago based on studies of S induced collisions at 200A GeV that rope formation leaves the absolute yield of produced kaons practically unmodified [11]. The situation does not change if collisions with heavy projectiles are considered (see table 3). The relative enhancement due to the weaker strangeness suppression is completely counterbalanced by the depletion of total multiplicity. The results in the DPM based string fusion approach SFMC confirm these conclusions and are surprisingly close to RQMD, even in terms of absolute numbers. The  $4\pi$  yields for central Pb on Pb collisions given in Ref. [23] are (with RQMD values in parantheses): negatively charged hadrons without fusion 924.4 (964.3), but with fusion included only 806.2 (829.2). In contrast, the kaon yields change much less,  $K^+$  90.1 versus 88.4 (79.2/79.0) and  $K^-$  71.5 versus 66.8 (53.0/50.4).

The  $R_s$  value increases in RQMD from 11.3 % to 15 % if the strings can fuse into color ropes and even to 24% if the hadrons interact with each other after formation. One can learn from these numbers that most of the strangeness enrichment is produced in the hadronic stage and not during the quark matter evolution in central Pb on Pb collisions. Furthermore, the strangeness enrichment in comparison to  $pp$  interactions is even stronger in central collisions with Pb than with S projectiles. Both aspects are actually connected as will be discussed in the following. The strangeness enhancement factor for quark pairs which are created in the rope field is practically projectile-independent in comparing central S and Pb collisions, namely 50 %. This is again a consequence of the finite energy and length scales which tend to suppress string excitations and longitudinal overlap of strings after the first 2-3 collisions of a colliding nucleon. Therefore the prehadronic processes are not responsible for the differences in the final states of reactions with S and Pb projectiles.

There are two reasons why the interactions in the hadronic stage are more

effective in enriching strangeness in reactions with larger projectile masses. The first reason is the increased stopping power which shifts relatively more nucleons of the target towards the central rapidity region. This allows them to participate more easily in interactions with secondaries which are concentrated around midrapidity. The prominent role of baryons in increasing the strangeness content of the system can be directly read off from table 3. The final baryons contain 124  $s$  valence quarks, which are 45 % of the  $s$  quarks created in total. A nuclear *hypermatter* state is created in these collisions according to the RQMD calculations. With respect to strangeness production, the dynamics of baryons is far from being a perturbation to the whole dynamics in  $AA$  reactions at the energy of 160A GeV.<sup>10</sup>

The second reason is related to the time intervals which the system spends in these two ‘phases’.<sup>11</sup> After the quark matter and hadronic preequilibrium stages which last about 3 (4) fm/c in S (Pb) induced reactions have been completed the system stays in approximate kinetic equilibrium for the rest of the interaction time. The temperature drops only slowly which is a property of the resonance gas with its many degrees of freedom. The hadrons and resonances interact in this stage until freeze-out, for approximately 11 fm/c in central Pb+Pb, but only for 3 fm/c in S+A reactions. Thus the weight of interactions in this third phase is more pronounced in Pb induced reactions than in light ion (e.g. O or S) collisions, even with heavy targets. In the latter case transverse expansion becomes rather effective after local kinetic equilibrium is reached, because the transverse area of the system is smaller.

## 4.4 Baryon pair production

A strong strange antibaryon enhancement has been experimentally observed for central S collisions on S and heavier targets [83, 84, 86]. Binary interactions in the rescattering stage tend to conserve particle numbers. This excludes them as an important contributor to the creation of additional antibaryons if the total interaction times are on the order of 4-6 fm/c only.

---

<sup>10</sup> Consideration of baryon degree of freedom is sometimes neglected in theoretical studies of  $AA$  collisions which is based on the small  $B/M$  ratio in the final state at 160-200A GeV. The important role of baryons for strangeness production which is found from RQMD has repercussions for the production of other particles whose production is inhibited by thresholds, for instance direct photons at large transverse momenta.

<sup>11</sup> A detailed account of the time evolution of the created matter in central Pb(160A GeV)+Pb collisions will be given elsewhere [15].



Such lifetimes of the interacting system in S+A collisions are suggested from interferometry data [87, 88] consistent with the RQMD calculations. The failure of Boltzmann-type hadron resonance gas dynamics to account for a sizable enhancement of strange antibaryons in central  $AA$  collisions points towards the importance of production mechanisms in denser stages of the reaction, notably in the prehadronic stage. This is supported by a simple argument. The energy needed to create a baryon pair is on the order of 2 to 3 GeV. Soft production processes which are characterized by the scale  $\Lambda_{QCD}^{-1} \approx 1\text{fm}$  therefore require energy densities of a few  $\text{GeV}/\text{fm}^3$  in order to overcome the  $B\bar{B}$  suppression in comparison to meson production.

Color ropes are a strong source of additional baryon pairs in ultrarelativistic  $AA$  collisions [11]. There are two distinct mechanisms how a rope may generate diquark pairs in the triplet representation ( $3 - \overline{QQ}$ ). These are quark coalescence in the rope end plates and quark pair creation with color mismatch in screening the field. The two processes are graphically represented in fig. 10. In the process of forming the rope charge elementary triplet charges of quarks and antiquarks in a receding rope ‘condensator’ plate couple stochastically to the total  $SU_3$  color charge of the rope. This provides a strong source of  $3 - \overline{QQ}$ ’s and  $\bar{3}-QQ$ ’s by quark coalescence. The statistical weight that two quarks form a  $\bar{3}-QQ$  compared to a  $6 - QQ$  is just 1:2. The (anti-)diquarks in triplet representation will combine with a corresponding anticharge to form an (anti-)baryon.

It turns out that in nuclear collisions at 160-200AGeV the probability of quark coalescence in the charge at the end of the rope is typically much larger (>90%) than due to diquark creation inside the field. This is very much based on the energy gain by optimal screening in course of charge creation  $\sim(C(p,q)-C(p,q-1))$  and/or  $\sim(C(p,q)-C(p-1,q))$  as compared to the nonoptimal case  $\sim(C(p,q)-C(p-1,q+1)+2/3)$ . Note that this result reflects also the rather short average length of the flux-tubes which are created at these energies. Giant flux-tubes with infinite length would be completely dominated by creation processes inside.

Indeed, baryon pair production is strongly increased in central Pb on Pb collisions if overlapping strings are fusing into ropes. The total number of created baryon pairs in the ‘NN mode’ turns out to be 27.7. Ropes increase this number to 84.3. The SFMC calculations show qualitatively similar trends, an increase (of  $2\bar{p}+\bar{\Lambda}$ ) from 16.7 to 83.9 due to string fusion [23]. However, the flavor dependence is different in the two approaches. In

RQMD the increase is strongest for strange antibaryons which is reflected for instance in the increase of the  $\bar{\Lambda}/\bar{p}$  ratio. The trend is the opposite in the SFMC results. The RQMD result arises from the ‘constructive interference’ of weaker strangeness suppression and additional diquark production mechanism if ropes are formed.

Subsequent antibaryon absorption in baryonic matter brings the final antibaryon yield from RQMD down again to 21.8 in the final state. This means that the strong antibaryon enhancement (a factor of 3) from the preequilibrium quark matter stage is more than ‘eaten up’ by the subsequent absorption in baryon-rich matter. Only a quarter of the initially produced antibaryons survives the interactions in the hadronic gas environment until freeze-out. Like in the case of strangeness enhancement a comparison of the yields in the different RQMD modes of operation demonstrates that the hadronic stage has much more impact on the flavor composition in central Pb+Pb than in S induced reactions [13]. The strength of the antibaryon absorption shows some flavor dependence. While the number of  $\bar{p}$  is even a factor of 2 below the results in the ‘NN mode’, the final yields of strange antibaryons are still considerably enhanced. For instance, the  $\bar{\Xi}$  yield increases by a factor of 7.7 compared to the result in the ‘NN mode’, even a factor of 13.3 if antibaryons would not be absorbed in the hadronic stage. Since both antibaryon and strangeness production are suppressed in elementary hadronic interactions, the rope formation effect is particularly strong for hadrons which carry these flavors in combination. Furthermore, the flavor dependence of antibaryon absorption reflects that  $s\bar{s}$  pairs are less frequent in the system and their annihilation probability is reduced, which mirrors the suppressed production probability (cf. section 3.2).

Is there some way to disentangle the antibaryon enhancement effect due to color rope formation or some other collective effect like QGP formation [89] in the early stage of the reaction from strong antibaryon absorption in the later hadronic stage? At least, it can be expected that the rather extreme model for antibaryon interactions adopted presently in RQMD which assumes a free  $\bar{p}p$  annihilation cross section can be tested rather well in heavy ion collisions. Since the annihilation cross section is strongly energy-dependent, preferentially low-momentum antibaryons are annihilated. This effect is even more pronounced in heavy ion collisions at lower beam energies [91]. The use of the free  $\bar{p}p$  annihilation cross section is certainly debatable [90], in particular at low relative momenta. Since this cross section corresponds

at low energy to particle interaction distances clearly larger than 1 fm and thus exceeds the inter-particle distance in the dense stage, medium effects are expected to be very important. The real part of the antibaryon self-energy in baryon-rich matter may get substantial values as well, because vector meson exchange leads to attraction in addition to attraction already from scalar exchange. It will have some influence on the shape of the particle spectra, although the magnitude of this effect is unclear [91].

## 5 Summary and Conclusions

String fusion into color ropes and hadronic rescattering – collective interactions in the preequilibrium quark matter and hadronic resonance gas stage of ultrarelativistic nucleus-nucleus collisions – have been modeled in RQMD. The system created in central Pb(160A GeV) on Pb reactions is characterized by strong longitudinal flow. The nucleon momentum distribution shows the strongest elongation along beam direction, but with a maximum still at midrapidity. The broadness arises from partial transparency (corona effect). The final antibaryon source is clearly more concentrated around midrapidity than their antiparticles, kaons and pions. Antibaryons are produced only in the region of highest energy density, while mesons and even strangeness are created also in the diluter regions as well. If these RQMD predictions are experimentally confirmed, strangeness and antibaryon enhancement in ultrarelativistic heavy ion collisions cannot be described by only one source with homogeneous flavor composition. The strangeness suppression factor defined by the ratio of created quark pairs  $s\bar{s}/(u\bar{u}+d\bar{d})$  is strongly enhanced by a factor of 2.4 in comparison to  $pp$  results. Color rope formation increases the initially produced yield of antibaryons to 3 times the value in the ‘NN mode’, and even stronger if they carry strangeness. Only approximately one quarter of the produced antibaryons survives because of subsequent strong absorption in baryon-rich matter. The differences in the final particle composition for Pb on Pb collisions to S induced reactions are attributed to the hadronic resonance gas stage which is baryon-richer and lasts longer in the heavy system.

## Acknowledgements

I acknowledge gratefully the help of M. Leltchouk, J. Nystrand, G. Heintzelman, M. Zou, and J. Nagle in eliminating some bugs in the computer code RQMD2.1 and getting it executable on various computers.

## Appendix: Quark pair creation in a rope

The path integral for the tunneling of a virtual charge pair is given in the WKB approximation as [92]:

$$P(p_t) = \left| e^{-2|S_{cl}|} \right|^2, \quad (26)$$

where  $S_{cl} = \int_0^{z_{fin}} p_l(z) dz$  is the action for the path across the classically forbidden region. Therefore longitudinal momentum and action  $S_{cl}$  are purely imaginary in this region, initially:

$$p_l^2 + p_t^2 + m^2 = 0 \quad . \quad (27)$$

The force acting on a created charge is given from the amount by which the field energy per unit-length is lowered due to screening of the original source [94]:

$$F_e = (\kappa - \kappa') \quad , \quad (28)$$

with  $\kappa$  the rope tension before and  $\kappa'$  the tension after pair creation. After each of the created charges has moved over a distance  $z$  the energy balance reads:

$$2F_e \cdot z = 2\sqrt{p_l^2(z) + p_t^2 + m^2} \quad , \quad (29)$$

for a charge with constant mass  $|S_{cl}| = \pi m_t^2/4(\kappa - \kappa')$ . However, it is assumed here that the mass varies linearly with distance which is motivated by the expectation that quark masses are ‘current’ on short distance scales and ‘constituent’ masses with respect to the nonperturbative confining force.

$$\begin{aligned} m(z) &= m_0 + \beta \cdot z, \\ z &\leq \Delta m/\beta \quad , \end{aligned} \quad (30)$$

with  $m_0$  the current quark mass ( $m_u = m_d = 10$  MeV,  $m_s = 160$  MeV),  $\Delta m=350$  MeV the difference to the constituent mass, and  $\beta=0.355$  GeV/fm the ‘speed’ of quark dressing. The parameters are fitted to give 0.1 for suppression of diquarks in comparison to quark production and 0.29 for strange

quark suppression in elementary flux-tube decays which are the values favored by experimental data.

The absolute value of the action  $S_{cl}$  for the tunneling of a quark with linear interpolation between current and constituent mass is given by

$$|S_{cl}| = I_1 + I_2, \quad (31)$$

$$I_1 = \frac{M^2}{2A} \cdot \left\{ \left( \frac{Az_1}{M} - \frac{\beta}{F_e} \right) \cdot \sqrt{1 - \left( \frac{Az_1}{M} - \frac{\beta}{F_e} \right)^2} + \frac{\beta}{F_e} \cdot \sqrt{1 - \left( \frac{\beta}{F_e} \right)^2} + \arcsin \left( \frac{Az_1}{M} - \frac{\beta}{F_e} \right) + \arcsin \left( \frac{\beta}{F_e} \right) \right\},$$

$$I_2 = \frac{z_2}{2} \cdot (m_{0t} + \Delta m) \cdot \Theta \left( m_{0t} - \Delta m \cdot \frac{F_e - \beta}{\beta} \right) \cdot \left( -\frac{\Delta m}{z_2 \cdot \beta} \cdot \sqrt{1 - \left( \frac{\Delta m}{z_2 \cdot \beta} \right)^2} + \frac{\pi}{2} - \arcsin \left( \frac{\Delta m}{z_2 \cdot \beta} \right) \right),$$

where the following abbreviations have been used:

$$A = \sqrt{F_e^2 - \beta^2}, \quad B = \frac{m_{0t} \cdot \beta}{A^2}, \quad M = m_{0t} \cdot \frac{F_e}{A},$$

$$z_1 = \text{Min} \left( \frac{\Delta M}{\beta}, \frac{m_{0t}}{F_e - \beta} \right), \quad z_2 = \frac{m_{0t} + \Delta m}{F_e}.$$

Casher, Neuberger and Nussinov (CNN) have rederived the exact Schwinger result for the vacuum persistence probability in the WKB approximation [51], with the additional benefit of getting out a transverse momentum distribution for the created charges. Following their derivation the pair production probability per unit-time and unit-volume in a uniform Abelian field is given by

$$\frac{d^4 p}{d^4 x} = \frac{\gamma}{4\pi^3} \cdot F_e \cdot \sum_{\text{flavors}} \sum_{n=1}^{\infty} \int d^2 p_t \frac{P(p_t)^n}{n}. \quad (32)$$

$\gamma$  denotes the degeneracy factor from the color degrees of freedom. In total there are  $2 \times 3=6$  different (anti-)quark color states. However, only three

of them can lower the field strength by screening a given rope charge (see fig. 11).

A charge vector in the  $SU_3$  multiplet  $(p,q)$  – with  $p \geq q$  for definiteness – could combine with a created (anti-)quark charge to a  $SU_3$  charge state in the multiplets  $(p,q-1)$ ,  $(p-1,q)$  or  $(p-1,q+1)$  to lower the field strength. One can see from fig. 11 that the sum of original  $SU_3$  charge and a color-‘up’ quark do not have only a nonzero component in the  $(p-1,q)$ , but also in the  $(p-1,q+1)$  multiplet. However, the latter possibility is discarded, because it is energetically unfavorable. Therefore the factor  $\gamma$  in the pair creation rate eq. (32) representing the color degree of freedom is set to 1 in the three cases given above ( $q \neq 0$  assumed). Screening of a color charge with  $q = 0$  can result in one state with charge  $(p-1,q)$  or in two states with charge  $(p-1,q+1)$  ( $\gamma=2$  in this case). The two configurations with screened charges in the  $(p,q-1)$ ,  $(p-1,q)$  multiplets will give  $3\bar{3}$  color singlet states together with the residual rope charge (optimal screening). The third configuration  $(p-1,q+1)$  consists of a  $\bar{3}$ -diquark on one side and an anti-diquark with opposite color charge on the other side (color mismatch) and possibly some other charge.

The color of a diquark created by screening  $(p,q) \rightarrow (p-1,q+1)$  will get neutralized in a next step by an additionally produced quark pair. This is the generalization of the 2-step process for baryon pair production in an elementary flux-tube [51] to the case of stronger chromoelectric fields. The model of diquarks adopted here resembles very much the picture which one gets from strong coupling QCD [93]. A baryon state is represented in configuration space as a system of three quarks, each of them connected to a junction, which couples them to a color singlet with the help of the Levi-Civita tensor  $\epsilon$  (Y-shaped string). An effective diquark carrying  $\bar{3}$ -color charge would consist of two quarks and the junction which should be treated as an additional dynamical degree of freedom in principle. In a diquark-creating tunneling process a piece of elementary color flux is replaced by the  $\epsilon$ -junction and two ‘legs’, each having half of the elementary string tension (from energy conservation). Thus the force creating a diquark pair in an elementary flux-tube is weaker by a factor 1/2 than the one which produces an optimally screening quark. This explains naturally the dynamical suppression of baryon pairs as compared to meson production in elementary flux-tube decays.

The produced quark pair acquires some transverse momentum in the tunneling process whose distribution can be calculated from eq. (32). However, one should not expect that a tube is straight and parallel to the distance

vector between source and sink of the electric field on a small distance scale since it is subject to ‘roughening’. Zero-point oscillations of a tube’s normal modes may provide another source of transverse momentum. Kokoski and Isgur discuss the effect of roughening for the breaking of a flux-tube in the strong-coupling limit [95]. On the other side, the effect should become irrelevant in the classical limit of infinite electrical field strength. Here I follow the pragmatic approach to add two uncorrelated components for a produced particle’s transverse momentum, one from tunneling and another one from unresolved transverse excitations which give for the absolute value:

$$p_{tr}^2 = p_0^2 + p_{tunn}^2 \quad . \quad (33)$$

The  $\vec{p}_0$  component is Gaussian distributed and fixed by the requirement that the total created transverse momentum in elementary flux-tube breaking is (approximately) 400 MeV.

## References

- [1] **Quark Matter ’95**, Proceedings of the 11<sup>th</sup> international conference on Quark Matter, Monterey, U.S.A., 1995. A.M. Poskanzer, J.W. Harris, and L.S. Schroeder, eds.: *Nucl. Phys.* **A590** (1995).
- [2] **Quark Matter ’93**, Proceedings of the 10<sup>th</sup> international conference on Quark Matter, Borlange, Sweden, 1993. E. Stenlund, H-A. Gustafsson, A. Oskarsson, and I. Otterlund, eds.: *Nucl. Phys.* **A566** (1994).
- [3] H. Sorge, H. Stöcker, and W. Greiner: *Ann. Phys. (N.Y.)* **192** (1989) 266; *Nucl. Phys.* **A498** (1989) 567c.
- [4] T.S. Biro, H.B. Nielsen, and J. Knoll: *Nucl. Phys.* **B245** (1984) 449.
- [5] G. Bertsch, S. DasGupta, and H. Kruse: *Phys. Rev.* **C 29** (1984) 673.
- [6] J. Aichelin, A. Rosenhauer, G. Peilert, H. Stöcker, and W. Greiner: *Phys. Rev. Lett.* **58** (1987) 1926.
- [7] J. Koplik, A.H. Mueller: *Phys. Rev.* **D 12** (1975) 3638.
- [8] A. Bialas, M. Bleszynski, and W. Czyz: *Nucl. Phys.* **B111** (1976) 461; A. Bialas, W. Czyz, and L. Lesniak: *Phys. Rev.* **D 25** (1982) 2328; *Z. f. Phys.* **C13** (1982) 147.

- [9] J. Nagle et al.: *Phys. Rev. Lett.* **73** (1994) 1219; 2417.
- [10] M. Gonin, O. Hansen, B. Moskowitz, F. Videbaek, H. Sorge, and R. Mattiello: *Phys. Rev. C* **51** (1995) 310.
- [11] H. Sorge, M. Berenguer, H. Stöcker, and W. Greiner: *Phys. Lett.* **B289** (1992) 6.
- [12] M. Berenguer, H. Sorge, and W. Greiner: *Phys. Lett.* **B332** (1994) 15.
- [13] H. Sorge: *Z. f. Phys.* **C67** (1995) 479.
- [14] H. Sorge: *Phys. Lett.* **B344** (1995) 35.
- [15] H. Sorge: to be published.
- [16] P. Koch, J. Rafelski, and B. Müller: *Phys. Rep.* **142** (1986) 167.
- [17] H. Sugauma, S. Sasaki, and H. Toki: *Nucl. Phys.* **B435** (1995) 207.
- [18] B. Nilsson-Almqvist, and E. Stenlund: *Comp. Phys. Comm.* **43** (1987) 387.
- [19] B. Andersson, G. Gustafson, G. Ingelman, and T. Sjöstrand: *Phys. Rep.* **97** (1983) 31.
- [20] K. Werner: *Phys. Rep.* **232** (1993) 87.
- [21] A. Capella, U. Sukhatme, C.-I. Tan, and J. Tran Thanh Van: *Phys. Rep.* **236** (1994) 346.
- [22] N. Amelin, M. Braun, and C. Pajares: *Phys. Lett.* **B306** (1993) 312.
- [23] N. Armesto, M.A. Braun, E.G. Ferreira, and C. Pajares: *Phys. Lett.* **B344** (1995) 301.
- [24] J. Aichelin, K. Werner: *Phys. Lett.* **B300** (1993) 158.
- [25] A. Capella: LPTHE 94-113 (preprint).
- [26] H. Sorge, R. Mattiello, H. Stöcker, and W. Greiner: *Phys. Lett.* **B271** (1991) 37.
- [27] M. Hofmann, R. Mattiello, H. Sorge, H. Stöcker, and W. Greiner: *Phys. Rev. C* **51** (1995) 2095.



- [28] T. Schlagel, S. Kahana, and Y. Pang: *Phys. Rev. Lett.* **69** (1992) 3290; *Nucl. Phys.* **A566** (1994) 465c.
- [29] J. Schaffner, I.N. Mishustin, L.M. Satarov, H. Stöcker, and W. Greiner: *Z. f. Phys.* **A341** (1991) 47.
- [30] C. M. Ko, M. Asakawa, and P. Levai: *Phys. Rev.* **C 46** (1992) 1072.
- [31] G. Wolf: *Prog. Part. Nucl. Phys.* **30** (1993) 273.
- [32] C. Hartnack, J. Jaenicke, and J. Aichelin: *Nucl. Phys.* **A580** (1994) 643.
- [33] H. Sorge, L. Winkelmann, H. Stöcker, and W. Greiner: *Z. f. Phys.* **C59** (1993) 85.
- [34] V.A. Abramovskii, V.N. Gribov, and O.V. Kancheli: *Sov. J. Nucl. Phys.* **18** 1974) 308.
- [35] H. Sorge: to be published.
- [36] A. Bialas, M. Gyulassy: *Nucl. Phys.* **B291** (1987) 793.
- [37] T. Sjöstrand: *Comp. Phys. Comm.* **39** (1986) 347.
- [38] P. Aurenche, F. W. Bopp, and J. Ranft: *Z. f. Phys.* **C23** (1984) 67.
- [39] K. Goulianos: *Phys. Rep.* **101** (1983) 169.
- [40] B. Andersson, G. Gustafson, and B. Nilsson-Almqvist: *Nucl. Phys.* **B281** (1987) 289.
- [41] A. Capella, J.A. Casado, C. Pajares, A. V. Ramello, and J. Tran Thanh Van: *Z. f. Phys.* **C33** (1987) 541.
- [42] J.T. Mitchell et al. (NA35 Collab.): *Nucl. Phys.* **A566** (1994) 415c.
- [43] R. C. Hwa: *Phys. Rev. Lett.* **52** (1984) 492; A. Klar, J. Hüfner: *Phys. Rev.* **D 31** (1985) 491; L. P. Csernai, J. I. Kapusta: *Phys. Rev.* **D 31** (1985) 2795.
- [44] D. Amati, A. Stanghellini, and S. Fubini: *Nuov. Cim.* **26** (1962) 6.
- [45] F.E. Low, K. Gottfried: *Phys. Rev.* **D 17** (1978) 2487.

- [46] C. Merino, C. Pajares, and J. Ranft: *Phys. Lett.* **B276** (1992) 168.
- [47] C. Bernard: *Phys. Lett.* **B108** (1982) 431, *Nucl. Phys.* **B219** (1983) 341; J. Ambjørn, P. Olesen, and C. Peterson: *Nucl. Phys.* **B240** (1984) 189; C. Michael: *Nucl. Phys.* **B259** (1985) 58; L.A. Griffiths, C. Michael, and P. Rakow: *Phys. Lett.* **B150** (1985) 196; N.A. Campbell, I.H. Jorjysz, and C. Michael: *Phys. Lett.* **B167** (1986) 91.
- [48] J. Kogut, L. Susskind: *Phys. Rev. D* **11** (1975) 395.
- [49] H.D. Trottier, R.M. Woloshyn: *Phys. Rev. D* **48** (1993) 2290.
- [50] J. Schwinger: *Phys. Rev.* **82** (1951) 664; E. Brezin, C. Itzykson: *Phys. Rev. D* **2** (1970) 1191.
- [51] A. Casher, H. Neuberger, and S. Nussinov: *Phys. Rev. D* **20** (1979) 179.
- [52] X. Artru, G. Mennessier: *Nucl. Phys.* **B70** (1974) 93.
- [53] M. Herrmann, J. Knoll: *Phys. Lett.* **B234** (1990) 437.
- [54] C. Martin, D. Vautherin: *Phys. Rev. D* **40** (1989) 1667.
- [55] A. Bialas, W. Czyz: *Nucl. Phys.* **B267** (1986) 242.
- [56] P.D.B. Collins: *Phys. Rep.* **4** (1971) 103.
- [57] S. Godfrey, N. Isgur: *Phys. Rev. D* **32** (1985) 1357.
- [58] B. R. Martin, D. Morgan, and G. Shaw: *Pion–Pion Interactions in Particle Physics*. Academic Press, London (1976).
- [59] K.T.R. Davies, M. Baranger: *Ann. Phys. (N.Y.)* **19** (1962) 383.
- [60] M. Berenguer: Ph. D. Thesis, Univ. Frankfurt (1994), unpublished.
- [61] Particle Data Group, K. Hikasa et al.: *Phys. Rev. D* **45** (1992).
- [62] N.P. Samios, M. Goldberg, and B.T. Meadows: *Rev. Mod. Phys.* **46** (1974) 49.
- [63] G. Veneziano: *Nuov. Cim.* **57A** (1968) 190.
- [64] J. Vandermeulen: *Z. f. Phys.* **C37** (1988) 563.

- [65] S. Mundigl, M. Vicente Vacas, and W. Weise: *Nucl. Phys.* **A523** (1991) 499.
- [66] P. Koch, C. Dover: *Phys. Rev.* **C 40** (1989) 145.
- [67] E. Ferrari, F. Selleri: *Phys. Rev. Lett.* **7** (1961) 387.
- [68] V. Dimitriev, O. Sushkov, and C. Gaarde: *Nucl. Phys.* **A459** (1986) 503.
- [69] J. Randrup, C.M. Ko: *Nucl. Phys.* **A343** (1980) 519.
- [70] R. Mattiello: Diploma Thesis, Univ. Frankfurt (1991), unpublished.
- [71] S. Gasierowicz: *Elementary Particle Physics*. John Wiley & Sons – New York (1966).
- [72] C.D. Frogatt, J.L. Petersen: *Nucl. Phys.* **B129** (1977) 89.
- [73] P. Estabrooks et al.: *Nucl. Phys.* **B133** (1978) 490.
- [74] D. Aston et al.: *Nucl. Phys.* **B296** (1988) 493.
- [75] J. Weinstein, N. Isgur: *Phys. Rev.* **D 41** (1990) 2236.
- [76] S.M. Flatté: *Phys. Lett.* **63B** (1976) 224.
- [77] S. Gavin, P. Ruuskanen: *Phys. Lett.* **B262** (1991) 326.
- [78] N.S. Amelin, E.F. Staubo, L.P. Csernai, V.D. Toneev, K.K. Gudima, and D. Strottman: *Phys. Lett.* **B261** (1991) 352.
- [79] K. Kadija, N. Schmitz, and P. Seyboth: MPI-PhE/95-07 (preprint), subm. to *Z. f. Phys.* **C**.
- [80] A. v. Keitz, L. Winckelmann, A. Jahns, H. Sorge, H. Stöcker, and W. Greiner: *Phys. Lett.* **B263** (1991) 353.
- [81] E. Schnedermann, J. Sollfrank, and U. Heinz: *Phys. Rev.* **C 48** (1993) 2462.
- [82] P. Braun-Munzinger et al.: *Phys. Lett.* **B344** (1995) 43.
- [83] J. Bartke et al. (NA35 Collab.): *Z. f. Phys.* **C48** (1990) 191.

- [84] J. Bächler et al. (NA35 Collab.): *Z. f. Phys.* **C61** (1994) 551.
- [85] K. Jaeger et al.: *Phys. Rev.* **D 11** (1975) 1756.
- [86] S. Abatzis et al. (WA85 Collab.): *Phys. Lett.* **B244** (1990) 130; *Phys. Lett.* **B259** (1990) 508; *Phys. Lett.* **B270** (1991) 123.
- [87] G. Roland et al. (NA35 Collab.): *Nucl. Phys.* **A566** (1994) 527c.
- [88] H. Beker et al. (NA44 Collab.): *Phys. Rev. Lett.* **74** (1995) 3340.
- [89] J. Letessier, J. Rafelski, and A. Tounsi: *Phys. Lett.* **B323** (1994) 393.
- [90] S.H. Kahana, Y. Pang, T. Schlagel, and C.B. Dover: *Phys. Rev.* **C 47** (1993) R1356.
- [91] C. Spieles, M. Bleicher, A. Jahns, R. Mattiello, H. Sorge, H. Stöcker, and W. Greiner: preprint UFTP 385-95, nucl-th/9506008, subm. to *Phys. Rev. C* (1995).
- [92] F.J. Yndurain: *Quantum Chromodynamics*, Springer, New York-Berlin-Heidelberg-Tokyo (1983).
- [93] J. Carlson, J. Kogut, and V.R. Pandharipande: *Phys. Rev.* **D 27** (1983) 233.
- [94] N.K. Glendenning, T. Matsui: *Phys. Rev.* **D 28** (1983) 2.
- [95] R. Kokoski, N. Isgur: *Phys. Rev.* **D 35** (1987) 907.

# Table Captions:

## Table 1:

Reggeon exchange in meson-baryon collisions: planar diagrams. The Reggeon which is exchanged in the various meson-baryon interactions describable by a planar quark-line diagram can be read off from the table. Values for intercept  $\alpha_R$ , strangeness and quark exchange suppression parameter  $r(R)$  and momentum parameter  $p_R$  are given here which enter into eq. (16).  $m$  denotes here a meson with strangeness  $S=0$ ,  $k$  with  $S=1$ , irrespectively which multiplet it belongs to. (In contrast, a  $K$  denotes a kaon and  $K^*$  a  $K^*(892)$ .) The multiplet of which an exchanged meson is a member is indicated by a  $V$  (vector) or  $PS$  (pseudoscalar meson nonet). Alternatively, the parameters are specified as some ‘average’ of the  $V$  and  $PS$  exchange parameters. Note that in the uppermost diagram the flow of isospin quantum numbers as specified and  $G$ -parity determine whether a  $V$  or a  $PS$  meson is exchanged.

## Table 2:

Reggeon exchange in meson-baryon collisions: exchange diagrams. Contrary to the Reggeon exchange diagrams in Table 1 the reactions tabelized here include a quark exchange between ingoing meson and baryon. The notation is the same as in Table 1.

## Table 3:

The produced hadronic state in Pb(160A GeV) on Pb collisions with impact parameters  $b < 1$  fm, calculated in three different operation modes of RQMD 2.1: so-called NN mode with ropes and rescattering switched off in the right column, rope fragmentation included in the middle column and ropes and hadronic rescattering both included in left column (default mode). All members of the pseudoscalar meson nonet and the baryon octet have been kept stable, except the  $\eta'(958)$  which is decaying already during the dynamical evolution generated by RQMD.

## Figure Captions:

### Figure 1:

Decaying hadronic string in position space (scaled by  $\kappa_{el}$ ). Four hadrons  $A-D$  are formed, their formation points indicated by dots. Thick lines give the trajectories along which the hadrons, respectively in the beginning the original constituent quarks, are propagated.  $p_L^+$ ,  $p_{Y_oY_o}^+$ , and  $p_B^+$  are the forward light cone momenta for the leading (spectator) quark, for string excitation and for the interacting (backward) quark.  $p_{T_a}^-$  is the backward light cone momentum which has been transferred from the target.

### Figure 2:

Schematic diagrams for string excitations in multiple baryon collisions: The primary string excitation is shown at the top (a). Either the interacting quark collides two or more times (c) or the spectator diquark of interaction (a) interacts (b). Iteration of diquark interaction is depicted in diagram (d). Here all original valence quarks are completely stripped off from the baryon which is emerging from the fragmentation process. Constituent quarks are symbolized by full dots (interacting quarks on left, spectators on right side), sea quark pairs by open circles. The ingoing light cone momenta – forward  $p_I$  ( $I$  for interaction) and  $p_S$  ( $S$  for spectator) and backward  $p_b$  (provided by the target) – are distributed onto outgoing constituents and string excitation ( $p_f-p_b$ ) as indicated just below each diagram.

### Figure 3:

Possible  $SU(3)$  multiplets which can be built by a combination of  $(p,q)$  states and elementary triplet (antitriplet) states.  $p$  is the number of columns with one line,  $q$  the number with two lines – ( $p=2$ ,  $q=2$  in this example). Thus  $p$  is the number of ‘quark-like’ charges,  $q$  of ‘antiquark-like’ charges. There is no restriction in *forming* the total rope charge. It is energetically allowed to create a charge in rope decay only if it screens the original rope charge, i.e. the resulting charge is lowered (right above, middle below and –  $p>q$  assumed – middle above). Thus only (at most) three out of six quark or antiquark states in color space can be created in the rope field.

### Figure 4:

Schematic picture of quark pair creation in a rope: quark trajectories are displayed in the  $t$ - $z$ -plane. The field strength is characterized by the  $(p,q)$  values of the source (which is acting here from the right side). It is indicated in the figure how charge creation and crossing of quark trajectories decrease the field strength inside the rope. Quark and antiquark may form a color singlet which splits from the rope (symbolized here by two horizontal lines). Two examples of hadron formation which are displayed here demonstrate that color is not necessarily locally confined in a rope field. Neighboring quark  $Q_d$  and antiquark  $\overline{Q_c}$  form a color singlet. Such a topology would be always enforced in elementary strings  $((p,q)=(1,0))$  by energy conservation. In contrast,  $\overline{Q_a}$  and  $Q_c$  travel quite some distance before they combine into a color singlet.

Figure 5:

Three mechanisms of chromoelectric field degradation: quark pair creation (a), turning point of a quark in the end plate source (b), and crossing point of two quark trajectories (c). The field strength is characterized by a pair of numbers like  $(p,q)$  which characterizes the charge acting from the right side. (The corresponding anticharge which is the sink of the flux on the left side is a member of the  $(q,p)$  multiplet.) Square brackets like  $[i,j]$  characterize the charge moving on a particular trajectory. While  $p$  and  $q$  can get assigned arbitrarily large integer values, a charge which is denoted by  $[i,j]$  in the diagrams belongs either to a triplet  $([1,0])$  or an antitriplet  $([0,1])$ .

Figure 6:

Phase shifts  $\delta_0^0$  and  $\delta_0^2$  in  $\pi\pi$  scattering: Comparison between calculation and experimental data. The data are taken from Refs. [72, 75].

Figure 7:

Rapidity distributions of negatively charged hadrons and net protons in Pb(160A GeV) on Pb collisions with impact parameters  $b < 1$  fm, calculated in three different operation modes of RQMD 2.1: ropes and rescattering switched off (dashed line), rope fragmentation included (dotted line) and ropes and hadronic rescattering both included which is the default mode (straight line). The rapidity is calculated in the equal-speed-system of projectile and target. The negatively charged hadrons include feed-down from weak decays (except from  $K_S$  and (anti-) $\Lambda$ ), the net protons from all weakly and strongly

unstable baryons.

Figure 8:

Rapidity distributions of strange baryons and kaons in central Pb(160AGeV) on Pb collisions. The different histograms are related to the different RQMD operation modes as explained in the caption to fig. 7. Note that the  $\Lambda$  distribution does not contain any feed-down from  $\Xi$  decay or  $\Sigma^0$ -decay. The  $\Sigma$ -rapidity distribution is calculated by averaging over all isospin states. The amount of splitting in the yields of the three states is small, however (see Table 3). The  $\Xi$  baryon distribution in the figure contains the sum of both charge states. Again, both states are populated approximately with equal strength.

Figure 9:

Rapidity distributions of anti-baryons ( $\bar{p}$ ,  $\bar{\Lambda}$ ,  $\bar{\Xi}$ ) in central Pb(160AGeV) on Pb collisions. The different histograms are related to the different RQMD modes of operation as explained in the caption to fig. 7. The  $\bar{\Xi}$  distribution contains the sum of both charge states. No feed-down from weak and electromagnetic decays is included.

Figure 10:

The two different production mechanisms of baryon pairs from rope fragmentation are depicted here schematically. An antiquark which is part of the original source charge of the color flux field may combine with an antiquark created by the field itself (left side). It is assumed here that the original charges making up the total rope charge move along the light cone. Having lost its momentum by pulling out the chromoelectric field an end plate charge turns its direction and gets accelerated again. After combining with a corresponding anticharge into a colorless state it will split from the rope without further interaction. This process is visualized here in the  $t$ - $z$  plane (with  $z$  the direction of the electric field). A flux tube may *create* as well a diquark-antidiquark pair in the color triplet configuration (right side). The scheme employed here is usually called two-step (or sometimes ‘popcorn’) production mechanism. It was first suggested in Ref. [51] for the case of baryon production from elementary flux tubes. The strength of the flux is indicated in the figure by a pair of numbers like  $(p,q)$  which defines the representation of the charge source. Note that the notation  $(\overline{QQ})_3$  to highlight



the quark content of the color charge means a (1,0) (or triplet) charge.

Figure 11:

The three configurations in color hypercharge and isospin space for screening of a charge in the multiplet  $(p,q)$  – here the state  $|(p,q),t=(p+q)/2,t^3=-t,y=(p-q)/3\rangle$  – by a created (anti-)quark charge. With  $p > q$  which is assumed here there is one screening antiquark color (a cross enclosed by a circle) and two quark colors (each represented by a cross).

Diagram (planar)	Subclasses/Examples	Reggeon	$2-2\alpha_R$	$r(R)$	$p_R$ (GeV)
	Isospin + G-parity } $0$ $0$ $0/I$ $I$	$V$ or $PS$	1 2	1	0.8
	$\bar{K}$ $\varrho$ $\bar{K}$ $\bar{K}^*$ $\pi$ $\bar{K}$ $\dots$	$V$  $PS$  $\overline{PS+V}$	1  2 1.5	1	0.8
	$K$ $\bar{K}^*$ $\pi$ $K^*(K)$ $\bar{K}$ $\pi(\varrho)$ $\dots$	$V$  $PS$  $\overline{PS+V}$	1.6  2.4 2.0	0.3	0.8

Table 1:

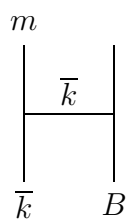
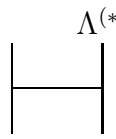
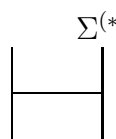
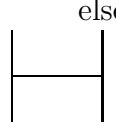
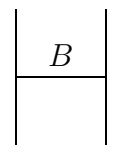
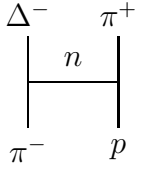
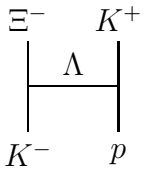
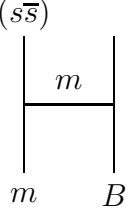
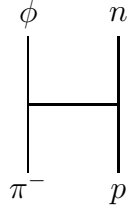
Diagram (exchange)	Subclasses/Examples	Reggeon	$2-2\alpha_R$	$r(R)$	$p_R$ (GeV)
	<p style="text-align: center;"><math>\Lambda^{(*)}</math></p>  <p style="text-align: center;"><math>\Sigma^{(*)}</math></p>  <p style="text-align: center;">else</p> 	<p style="text-align: center;"><math>PS</math></p> <p style="text-align: center;"><math>V</math></p> <p style="text-align: center;"><math>\overline{PS+V}</math></p>	<p style="text-align: center;">2.4</p> <p style="text-align: center;">1.6</p> <p style="text-align: center;">2.0</p>	<p style="text-align: center;">0.5</p>	<p style="text-align: center;">0.8</p>
	<p style="text-align: center;"><math>\Delta^- \quad \pi^+</math></p>  <p style="text-align: center;"><math>\Xi^- \quad K^+</math></p> 	<p style="text-align: center;"><math>N</math></p> <p style="text-align: center;"><math>Y/\Xi</math></p>	<p style="text-align: center;">2.8</p> <p style="text-align: center;">3.8</p>	<p style="text-align: center;">0.5</p> <p style="text-align: center;">0.3</p>	<p style="text-align: center;">1.4</p>
<p style="text-align: center;"><math>(s\bar{s})</math></p> 	<p style="text-align: center;"><math>\phi \quad n</math></p> 		<p style="text-align: center;">3.8</p>	<p style="text-align: center;">0.09</p>	<p style="text-align: center;">1.4</p>

Table 2:

	Ropes + Rescattering	Ropes + no Rescattering	no Ropes + no Rescattering
$p$	157.8	199.7	184.5
$n$	161.4	217.6	204.9
$\Lambda$	48.7	35.3	26.0
$\Sigma^+$	17.7	12.9	7.6
$\Sigma^0$	17.8	13.1	8.0
$\Sigma^-$	17.9	13.3	8.3
$\Xi^0$	5.4	4.2	2.1
$\Xi^-$	5.4	4.2	2.0
$\bar{p}$	5.6	27.9	11.3
$\bar{n}$	5.6	27.9	11.4
$\bar{\Lambda}$	3.8	10.7	2.3
$\bar{\Sigma}^+$	1.5	4.6	0.8
$\bar{\Sigma}^0$	1.5	4.6	0.8
$\bar{\Sigma}^-$	1.5	4.6	0.8
$\bar{\Xi}^0$	1.1	2.0	0.1
$\bar{\Xi}^-$	1.2	2.0	0.2
$\pi^+$	642.7	692.9	856.2
$\pi^0$	678.7	724.9	884.2
$\pi^-$	680.3	728.8	888.9
$K^+$	130.3	79.0	79.2
$K^-$	75.4	50.4	53.0
$K_s+K_l$	200.6	127.0	132.1
$\eta$	81.7	84.7	86.7

Table 3:

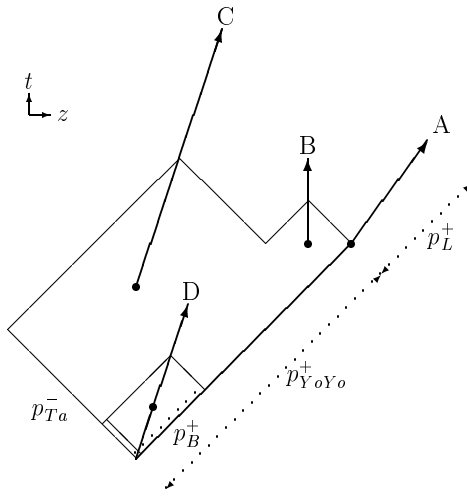


Figure 1:

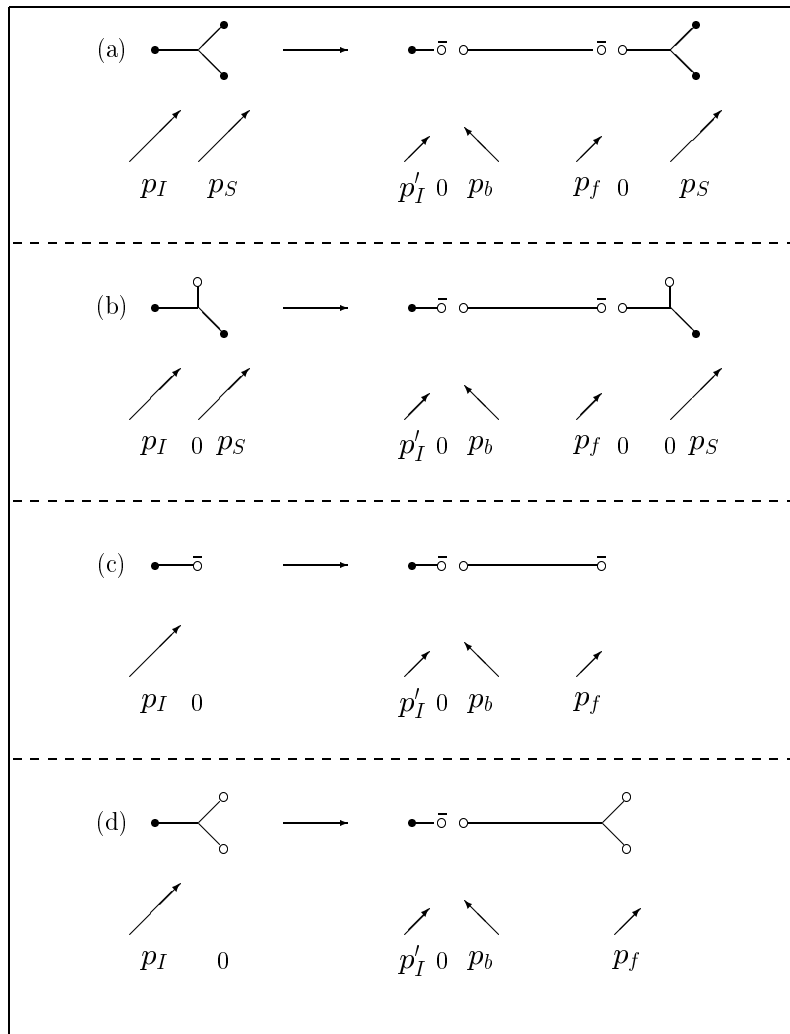
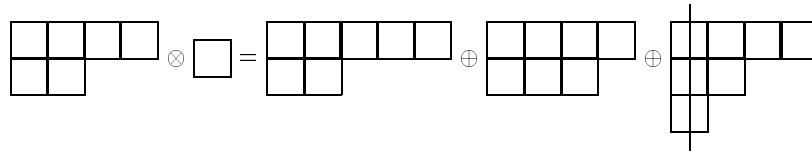
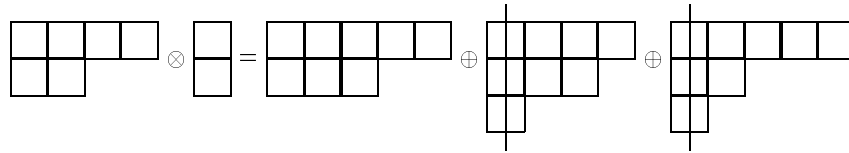


Figure 2:



$$(p, q) \otimes (1, 0) = (p+1, q) \oplus (p-1, q+1) \oplus (p, q-1)$$



$$(p, q) \otimes (0, 1) = (p, q+1) \oplus (p-1, q) \oplus (p+1, q-1)$$

Figure 3:

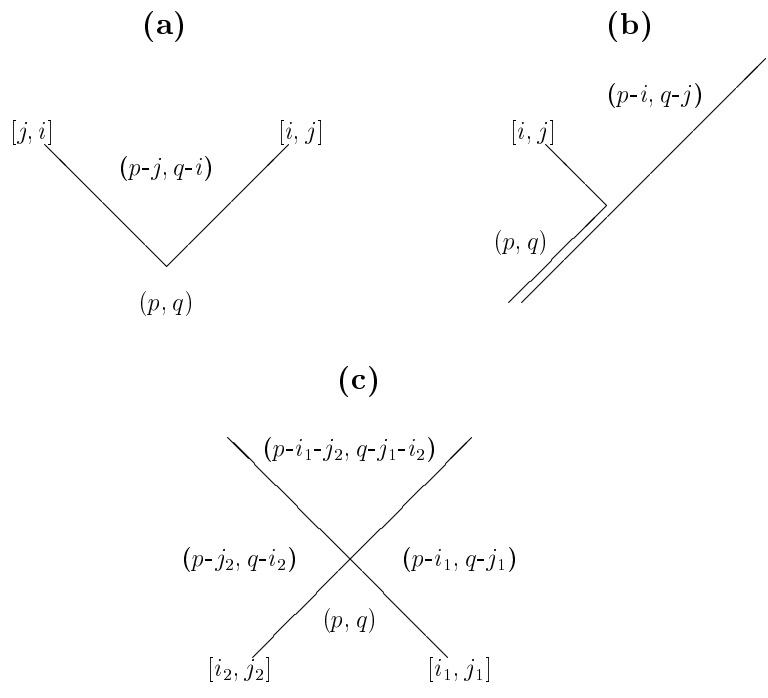


Figure 4:



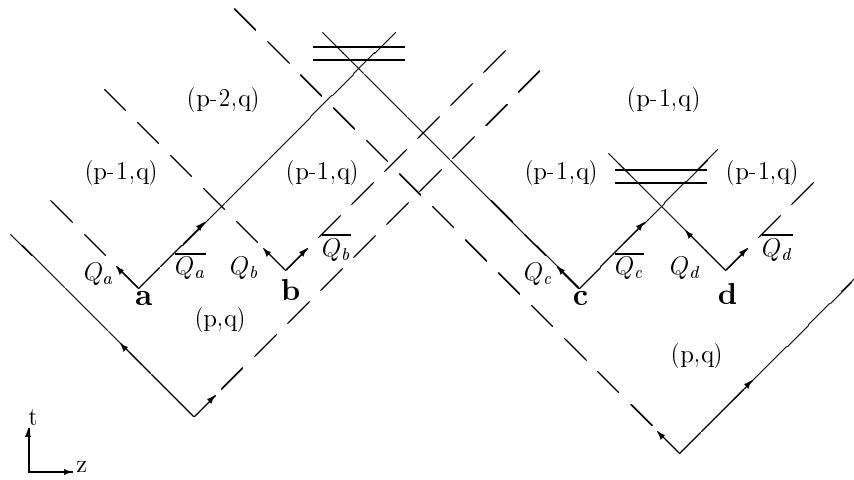


Figure 5:

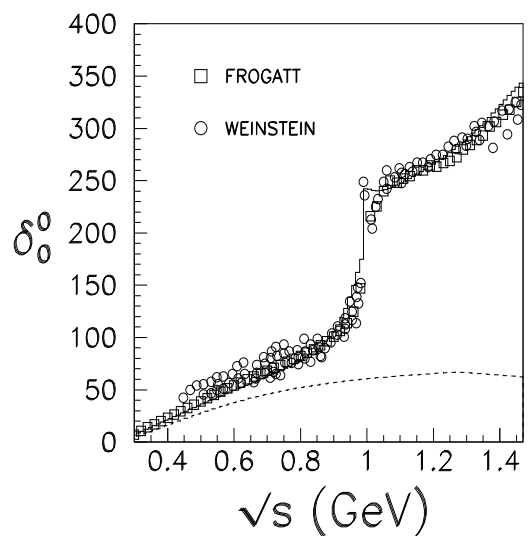
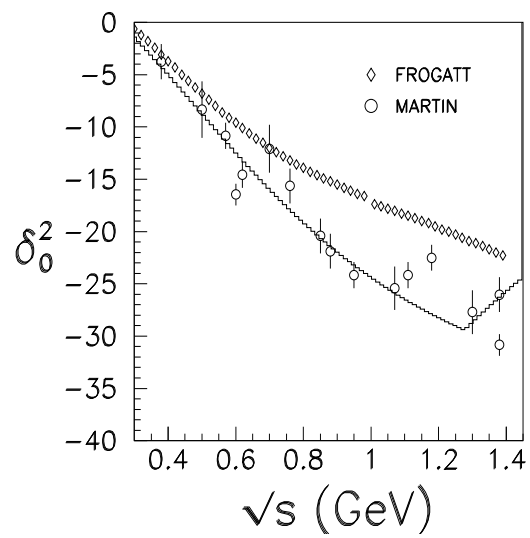


Figure 6:

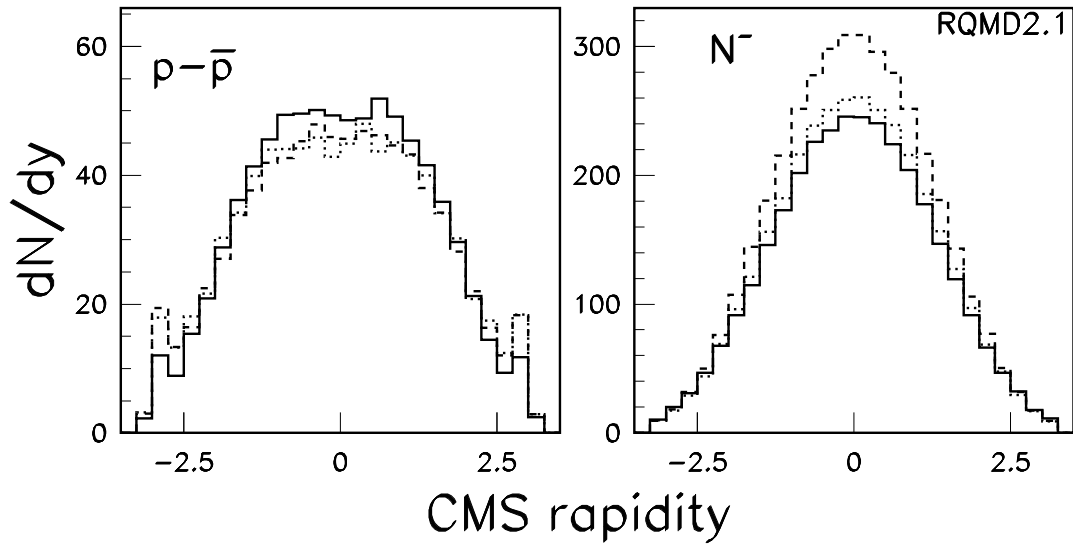


Figure 7:

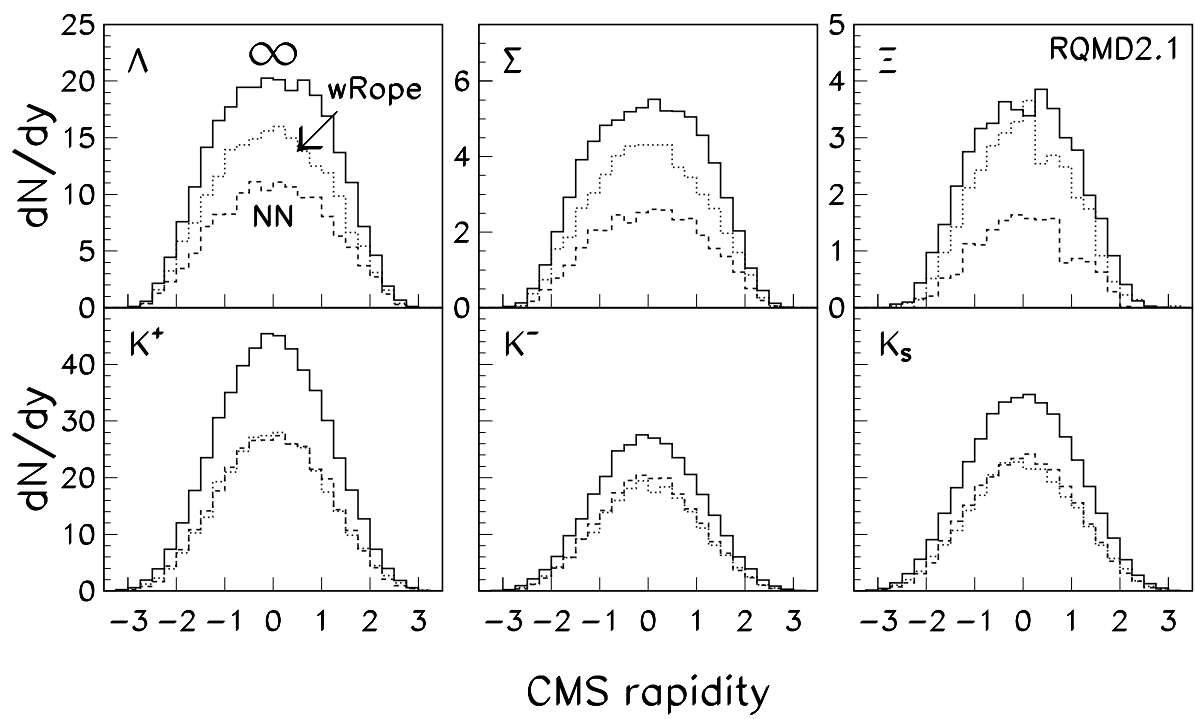


Figure 8:

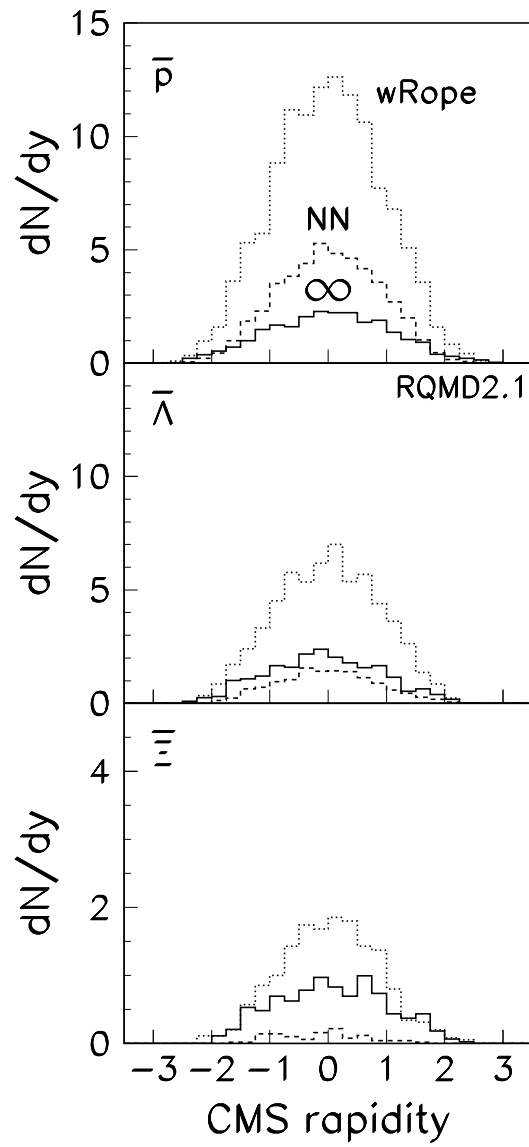
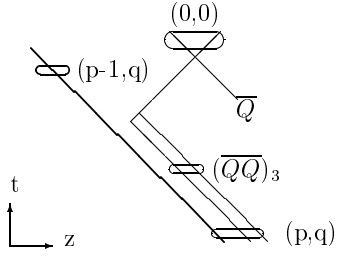


Figure 9:

$(\overline{QQ})_3$  formation

(a) in rope end 'plate'



(b) in rope interior

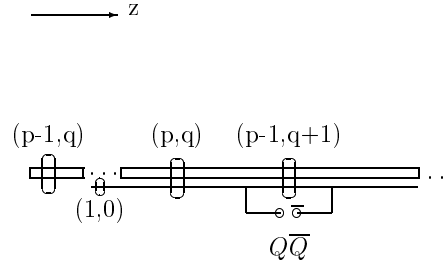


Figure 10:

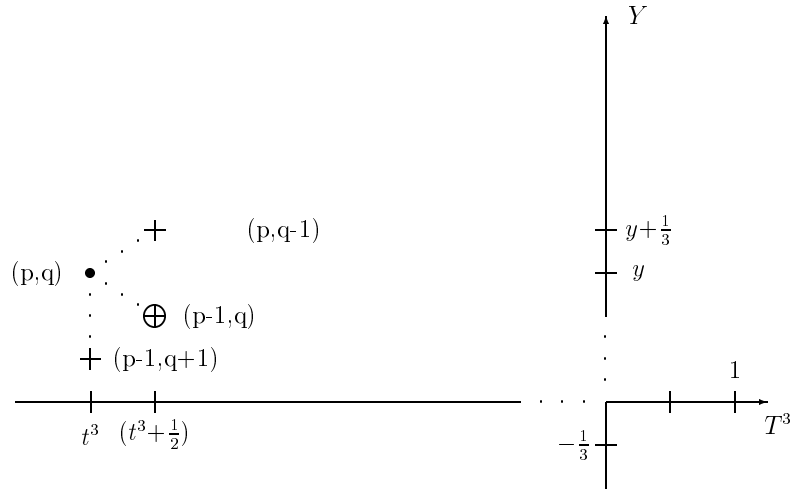


Figure 11: